MESH ADAPTATION IN FRACTURED RESERVOIR SIMULATION

A THESIS IN

Mathematics

Presented to the Faculty of the University

of Missouri-Kansas City in partial fulfillment of

the requirements for the degree

MASTER OF SCIENCE

by

Ahmed Azeez

B.A. Mathematics, Tikrit University, 2010

Kansas City, Missouri

2017

MESH ADAPTATION IN FRACTURED RESERVOIR SIMULATION

Ahmed Azeez, Candidate for the Master of Science Degree

University of Missouri-Kansas City, 2017

ABSTRACT

Natural fractures exist in many oil and gas reservoirs. On the other hand, hydraulic fracturing (fracking) is needed to create fractures in some reservoirs to improve the production rate. For example, shale gas reservoirs typically have extremely low permeability but have become an attractive source for natural gas production largely due to the advancement of horizontal drilling and hydraulic fracturing techniques. The permeability in fractures are much higher than that in other parts of the reservoir but the sizes of the fractures are much smaller. Thus, it is desirable to place more mesh elements around the fractures during the simulation and computations.

Mesh adaptation is a very useful technique to help improving the accuracy and efficiency of the computation, and can be applied in computations for many problems such as plasma physics, image processing, and reservoir simulation in petroleum engineering. This study will focus on mesh adaptation in fractured reservoir simulation. The mesh will be adapted automatically so that more elements are concentrated around the fractures and less elements are distributed in other places. By this way, the reservoir simulation can be more accurate and efficient which is critical in helping control the production rate, optimize hydraulic fracturing design, and evaluate enhanced oil recovery processes. The goal of this study is to evaluate the effects of different mesh adaptation methods when solving a partial differential equation called porous media equation (PME).

The porous media equation is solved using Finite Element Method with the software FreeFem++ that has built-in mesh adaptation functionality. The mesh is adapted based on a metric tensor that determines the shape, size and orientation of the mesh elements. The results are compared with uniform meshes and meshes created based on log-spacing. The numerical results show that adaptive meshes based on metric tensor provide the best results.

APPROVAL PAGE

The faculty listed below, appointed by the Dean of the College of Arts and Sciences, have examined a thesis titled “Mesh Adaptation in Fractured Reservoir Simulation” presented by Ahmed Azeez, candidate for the Master of Science degree, and certify that in their opinion it is worthy of acceptance.

Supervisory Committee

Xianping Li, Ph.D., Committee Chair

Department of Mathematics and Statistics

Noah Rhee, Ph.D., Committee Member

Department of Mathematics and Statistics

Majid Bani-Yaghoub, Ph.D., Committee Member

Department of Mathematics and Statistics

CONTENTS

LIST OF TABLES

LIST OF ILLUSTRATIONS

ACKNOWLEDGEMENTS

Foremost, I am thankful to the most gracious and the beneficent God for his countless blessings on me.

I would like to express sincere appreciation to my advisor Professor Xianping Li for his sagacious guidance and inspiring encouragement throughout my master study in Mathematics. Without his grateful support, I would never have completed this degree.

I owe my deepest gratitude to my parents, for their love, support and appreciation over the period of my studies.

I would like to thank my wife Amani for her unwavering support over the last three years. She was always there to bounce my ideas off and to give me a quick kick in the pants whenever I appeared to be slacking off.

CHAPTER 1

INTRODUCTION

In this chapter, we first give a brief introduction about fluid flow in fractured reservoirs and discuss the motivation for choosing this topic. Then, the overall structure of the thesis is given.

1.1 Background

The fluid flow mechanism through naturally fractured reservoirs are not well understood due to the involvement of complicated mass transfer between two different media. Also, it is challenging to computationally simulate the flow through fractured media due to the arbitrary orientation of natural fractures and their different lengths and sizes inside the reservoir.

The importance of flow and transport process in fractured rock to underground natural-resource recovery, waste storage and environmental remediation have motivated many studies, and significant progress have been achieved toward the modelling [1]. However, the conceptual and mathematical challenge to model the coupled processes of multiphase fluid flow, heat transfer and migration of chemical species in a fractured porous medium is still far from being overcome. The challenges are threefold (1) the nature of inherent heterogeneity, (2) the characterization of a fractured matrix system in a reservoir has many uncertainties, and (3) the flow and transport process in these systems are difficult to describe and understand. Dual porosity/permeability, discrete fracture approach and hybrid scheme are among the popular approaches used to model fluid flow through naturally fractured reservoirs.

In dual porosity/permeability approach, matrix and fracture are two layers with infinite length, they are parallel, and considered as two interacting continua. The dual porosity/permeability approach goes through developing conceptual models, that contain information on the geometry of the fracture-matrix system, as well as establishing the equations of the general mass and energy conservation for overlapping fracture matrix domains. Analytically or numerically solving the governing equations that couple fluid and heat is the main focus. The way of interaction of matrix and fracture under different reservoir conditions is the main issue in simulating flow and transport in fractured rock. Usually, dealing with this issue requires (1) an explicit discrete fracture and matrix model [2], (2) the dual continuum methods including double- and multi-porosity, dual permeability, or the more general "multiple interacting continua" (MINC) method (e.g., [1]and [3]), and (3) the effective continua method (ECM) [4]. Assuming a very simplified geometrical representation of matrix and fracture is the main disadvantage of this approach.

1.2 Motivation

There are many physical applications for this simple model because porous media equation (PME) can describe fluid flow, heat transfer or diffusion. Early applications for PME include groundwater infiltration by Boussisnesq in 1903 [5], and gas flow through a porous medium by Leibenzon and Muskat [6]. Heat radiation in plasmas is another important application for PME.

Petroleum engineering is an important field that present anisotropic diffusion. The world's need for gas and oil are not met despite the large quantities produced on a daily basis. The study of production of gas reservoirs in complicated geologic formations and sea beds is a hot topic.

Fluid flow in porous media (an interconnected network of pores filled with a fluid permeated in a material) in geologic formation is an important topic in gas and oil production.

Extracting crude oil and natural gas from porous media in geologic formation is a big part of petroleum engineering. The properties of the rock such as porosity, permeability, adhesion and reaction with the fluid are factors that control the flow of the fluid (water, oil, or gas). Porosity is the ratio of the space of pores to the total volume of the rock. There are two types of pores, isolated and interconnected. Only the fluid from interconnected pores can be produced out, thus porosity is the capacity of the reservoir rock to store producible fluid in its pores. To determine the porosity, the measurement of the volume of interconnected pores to the volume of the rock is necessary, which is called effective porosity. The transmission of fluid in a porous medium through the interconnected pores is called permeability. The terms absolute permeability or permeability are used interchangeably if the medium is saturated with a single liquid phase. If the medium contains multiple liquid phases, then each fluid phase has permeability called effective permeability which is the permeability of the porous medium to that particular fluid phase. Many factors affect the permeability, such as location and direction of the fluid. Both the porosity and permeability can be independent of the location, in this case, the reservoir rock is called homogenous in that property, or heterogeneous in that property if said property is dependent on the location. For example, a reservoir can be heterogeneous in porosity but homogenous in permeability. The porous medium is isotropic or anisotropic if said property is independent or dependent of the direction of the flow respectively.

1.3 Thesis Structure

The frame work of the thesis is as follows. In Chapter 2, we discuss porous media equation and its properties. Different types of fractures in fractured reservoirs are also described. Chapter 3

gives a brief explanation about finite element method and numerical solutions. Mesh adaptation and FreeFem++ software are also introduced. Numerical results for PME in 1D and 2D without and with fractures are presented in Chapter 4. Finally, some conclusions are drawn in chapter 5.

CHAPTER 2

POROUS MEDIA EQUATION AND FRACTURED RESERVOIRS

In this chapter we discuss porous media equation (PME) and fractured reservoirs. In Section 2.1, we explain what is PME and how PME could be considered as a nonlinear parabolic equation. Also, we give some properties of PME. We talk about how gas flows through a porous medium. Finally, we talk about Darcy's Law and permeability. In the Section 2.2, we discuss some details about fractured reservoirs and describe the types of fractures. Finally, we talk about Pseudo Steady State Models, Unsteady State Models and Linear Flow in fractured reservoirs.

2.1 Porous Media Equation

In this section, we try to present a systematic presentation of the mathematical theory of the nonlinear heat equation:

$$\text{(PME)} \ldots. \ \partial_t u = \Delta u^{m+1} \qquad m > 0. \qquad (2.1)$$

The equation above is called the Porous Medium Equation, with due attention paid to closest relatives. This equation has default settings which are the nonnegative scalar function $u = u(x,t)$ of space $x \in R^d$ *and* $t \in R$, with a space dimension $d \geq 1$, and $m > 1$. Δ is the Laplace operator. As an abbreviation, we will refer to the above equation as PME in the rest of this thesis. The PME equation is defined for all $x \in R^d$ and $0 < t < \infty$. To obtain the solution, we first need to

initialize the equation with some conditions. However, in practical problems, the PME equation is posed in a bounded subdomain [7] Ω contained in R^d for $0 < t < T$, and finding the unique solution requires boundary and initial conditions [8].

2.1.1 Development of PME

Henry Darcy conducted the fundamental experiment, hence the name Darcy's Law, which exists in various formulations. Darcy selected different soil samples for a particular difference in piezometric height, and measured the flow through them. The conclusion that he laid out is that the averaged flux is proportional to a permeability coefficient multiplied by the ratio of the difference in piezometric height to the distance [7]. The piezometric difference in height can be transformed to a pressure difference by simply multiplying by the fluid density and the gravitational constant. Darcy's Law can be formulated as follows in the case where the ratio of the difference in pressure and the distance are expressed continuously:

$$u = -K\nabla p, \qquad (2.2)$$

where u is called the Darcy velocity, which is the vector field of the mean flux averaged over the cross-sectional area, K is the permeability tensor and p is the fluid pressure. To be more precise, the permeability tensor is the hydraulic conductivity of the system in this formulation. In the case of single fluid phase:

$$K = \frac{\rho \tilde{g}}{\tilde{\mu}} \widetilde{K}, \qquad (2.3)$$

with ρ being the fluid density, $\tilde{g}$ the gravitational constant, $\tilde{\mu}$ the dynamic viscosity and $\widetilde{K}$, the intrinsic permeability tensor. The latter is independent of the fluid because it is a property of the

porous medium, meaning it speaks to the directional resistance of the porous medium to the flow. The permeability is uniform in all spatial directions in the case of an isotropic porous medium.

The parameter *K* is solely a property of the porous medium and is denoted as the intrinsic permeability because of the disconnection of the effects of the fluid and the solid matrix. Since the porous medium is often not homogenous, the permeability is written in tensor form generally as follows

$$K = \begin{bmatrix} k_{xx} & k_{xy} & k_{xz} \\ k_{yx} & k_{yy} & k_{yz} \\ k_{zx} & k_{zy} & k_{zz} \end{bmatrix}.$$

The resistance to the fluid flow varies with the spatial direction because the grains are naturally in a layered configuration and not well sorted or uniformly shaped. The property of non-uniform permeability is stronger for fractures, caused by their genesis from well-defined stress tensors. However, with fundamental setups, we do not consider the three-dimensional orientations of the soil grains nor do we consider the fractures, using a uniform scalar permeability: [9]

$$K = \begin{bmatrix} k_{xx} & 0 & 0 \\ 0 & k_{yy} & 0 \\ 0 & 0 & k_{zz} \end{bmatrix} \quad with\ k_{xx} = k_{yy} = k_{zz} \qquad (2.4)$$

Nevertheless, we account for most of certain flow directions within the fracture because a harmonic averaging technique is applied for the permeability.

$$K_{\ average} = \frac{n}{\sum_{i=0}^{n} K_i}\,. \qquad (2.5)$$

So, flow from fracture over the fracture-matrix interface is increased by neighboring nodes of the matrix causing a higher resistance.

The name of the Porous Medium Equation comes from the fact that it is used to describe the flow of an ideal gas in a homogenous porous medium. We can formulate the flow starting from a macroscopic point of view in terms of the functions of space *x* and time *t*, the density ρ, pressure *p*, and the velocity *V* according to [10] [6]. The previous quantities are linked together by

(i) the mass balance (also called the continuity equation by fluid mechanics),

$$\epsilon\rho_t + \nabla \cdot (\rho V) = 0 \qquad (2.6)$$

$where\ \epsilon \in (0,1)$ is the porosity of the medium, and $\nabla \cdot$ is the divergence operator.

(ii) the Darcy's Law,

$$\mu V = -K\nabla p \qquad (2.7)$$

It is an empirical law introduced by the French engineer H. Darcy [7] that describes the dynamic of flows through porous media.

(iii) the State equation

$$p = p_0\rho^{\gamma} \qquad (2.8),$$

with γ being the polytropic exponent. When applied to gases, and depending on the two-state law, it has two values: $\gamma = 1$ for isothermal processes, and for adiabatic one's γ is greater than 1. All the parameters including the permeability, the viscosity, the reference pressure, and the porosity are assumed to be positive constants, which are motivated by an admissible simplification in many

practical examples. However, that should not be the case in more general instances. Adopting such a hypothesis allows us to reduce (2.6) - (2.8) to the following form:

$$\rho_t = c\nabla \cdot (k\rho^m \nabla\rho) \qquad (2.9)$$

with exponent $m = 1 + \gamma$ and

$$c = \frac{\gamma p_0}{(\gamma+1)\varepsilon\mu}.$$

We can scale the time variable to get rid of the constant *c* to obtain the PME. It is well known in Mathematics that the constant can be easily scaled out to have no role, on the other hand, the engineers will still want to examine them.

It is straightforward to realize that the exponent m in the applications above is equal or larger than 2. Not many differences between the exponents m are found in the mathematical theory to be developed below as long as they are larger than 1, despite that the formula is simpler for *m=2*. The divergence ($\nabla\cdot$), gradient (∇) and Laplacian (Δ) operators act on the space variable $x = (x_1, \ldots, x_d)$. As an effort to adapt to the new usage in the PME, we will update our notation to the following: for the density, we will use the letter u instead of ρ, and for the pressure we will use the letter *v*, the pressure is defined as

$$v = \frac{m}{m-1} u^{m-1} \qquad (2.10)$$

The above expression is called the mathematician's pressure, which allows for an easy recovery of the above physical formulas with $\varepsilon = \mu = 1$. Now we can deduce Darcy's Law for the velocity as follows:

$$V = -k\nabla v = -m\, k\, u^{m-2}\nabla u \qquad (2.11)$$

We can also write the mass balance as follows $\partial_t u + \nabla \cdot j = 0, \quad j = uV$ is called the mass flux. The PME is

$$\partial_t u = \nabla \cdot (k u^m \nabla u) \qquad (2.12)$$

2.1.2 The PME as a Nonlinear Parabolic Equation

The PME is a simpler nonlinear version of the classical heat equation, and is a nonlinear evolution equation of parabolic type. The complete version in diversion form is:

$$\partial_t u = \nabla \cdot (D(u) \nabla u) + f , \qquad (2.13)$$

Assuming $u \geq 0$ the diffusion coefficient *D(u)* of the PME equals mku^{m-1}, we can also see that for signed solutions ($D(u) = m|u|^{m-1}$ in the modified form) the $D(u) = |u|^{m-1}$. The PME is a degenerate parabolic equation since it is parabolic only where $u \neq 0$ while the disappearance of D(u) suggests that the PME degenerates wherever $u = 0$.

It is well known that divergence form of equations deals with the category of nonlinear parabolic equations of the form:

$$\partial_t u = \nabla \cdot A(x, t, u, Du) + B(x, t, u, Du). \qquad (2.14)$$

With the vector function $A = (A_1, \ldots, A_d)$ satisfying both suitable structural assumptions and elliptical conditions, and the scalar function *B* satisfying only the suitable structural assumptions. In the second half of the last century the tools of functional analysis became available, which led to an increased interest for this research topic in PDEs. The extension of the theory can accommodate systems of similar form, where $u = (u_1, \ldots, u_k)$ is a vector variable, *A* is an *(m,d)* matrix and *B* is an *m*-vector. The generalization includes well established areas such as Reaction-

diffusion. Many literatures talk about this topic such as [11] [12] [13]. At the level of $u = 0$, we can demonstrate the change of character of the PME through performing the calculation of the Laplacian of the power function in the case $m=2$; assuming $u \geq 0$, the form results in

$$\partial_t u = 2u\Delta u + 2|\nabla u|^2. \qquad (2.15)$$

Notice that the leading term in the right-hand side, the region where $u \neq 0$, is the Laplacian modified by the variable coefficient $2u$; on the other hand, where $u \to 0$, the equation simplifies to $\partial_t u \sim 2|\nabla u|^2$ the Eikonal equation (a first order equation of Hamilton-Jacobi type that propagates along characteristics). Once we introduce a term called the pressure variable $v = cu^{m-1}$ for some $c \geq 0$, we can also conduct similar calculations for $m \neq 1$. Then equation

$$\partial_t v = av\Delta v + b|\nabla v|^2 \qquad (2.16)$$

can be obtained, with $a = m/c$, $b = m/(c(m-1))$. Similar conclusions about the behavior of the equation for $u, v \sim 0$ when $m \neq 2$ can be obtained through this fundamental transformation in the theory of PME. c is usually chosen to be equal to $\frac{m}{m-1}$ for the sole reason that it simplifies the formula $(a = m-1, b=1)$ as well as it makes sense for dynamical consideration, but c is also used. It should be noted that, mathematically speaking, the choice of the constant is not crucial. Note that similar consideration applies to the PDE but then

$$D(u) = \frac{m}{|u|^{1-m}} \to \infty \; as \; u \to 0. \qquad (2.17)$$

As a consequence, the name of fast diffusion is well deserved. The pressure can be introduced to a different role than in the PME because it is an inverse power of u, thus the differences and kinship between the two equations. Being a nonlinear and degenerate equation, the mathematical theory

for the PME was developed slowly despite its simplicity and important applications. Some of the basic techniques are not challenging nor they are computationally intensive although they originate from the linear methods used in dealing with heat equation. Many other nonlinear PDE's of parabolic type can be studied using these equations. In a broader scope, the reader can gain an insight to the nonlinear science from the study of the PME, such as the existence of free boundaries, the occurrence of limited regularity, and interesting asymptotic behavior.

2.1.3 Properties of the PME

The PME is different than the parabolic equation in that it provides some special traits that are not in the parabolic theory. Mathematically, the fact that D(u) is not always positive raises challenges. To account for the main qualitative difference, we introduce the dynamical concept, a property called the finite propagation. This property is in a strong disagreement with a well-known property of the classical heat equation, the infinite speed of propagation, one of the most contested aspects of the heat equation on physical grounds. "A nonnegative solution of the heat equation is automatically positive everywhere in its domain of definition" where "disturbances from the level $u = 0$ propagate in time with finite speed for solutions of the porous medium equation".

The physical sense of the PME to model diffusion or heat propagation is supported by the property of finite propagation. The strong maximum principle cannot hold as a consequence of the finite propagation property of the theory of the PME. The advantages are that as long as the initial values are zero in certain open domain of the space, a free boundary that separates the regions where the solution is positive appears due to the property of finite propagation, from the empty region where $u=0$. Precisely, the free boundary is defined as $\Gamma = \partial P_u \cap Q$, where Q is the domain of definition of the solution in space-time, $p_u = \{(x,t) \in Q : u(x,t) > 0\}$ is the positively set, and

∂ denotes the boundary. It is also called the moving boundary due to the fact that it moves as time evolves. The name interface is also commonly used for moving boundary.

A crucial and challenging topic of the mathematical investigation is the propagation fronts or the theory of free boundaries [14] . In principle, the free boundary of a nonlinear problem is an extremely complicated closed subset of *Q*. To prove that it is at least a Holder continuous (C^{α}) hypersurface in R^{d+1} and to investigate its smoothness is a real problem of the PME theory. Let us assume that it is often C^{∞}smooth. Two main scenarios will be faced. The first one is, R^{d} is the space domain, the initial data u_0 have compact support. In that case, the solution *u(x, t)* outside a compact set that changes with time [8] vanishes. Define the positive set at time *t* as

$$P_u = \{x \in R^d : u(x,t) > 0\}$$

and the support at time *t* as $S_u(t)$ that is the closure of $P_u(t)$. Then both of the bounded sets will expand in time. In the second scenario, the initial configuration 'has a hole in the support'. Then the solution contains a potentially smaller hole for t greater than zero. The focusing problem, one of the most celebrated mathematical developments of the PME theory, is motivated by the fact that the hole does disappear in finite time.

2.1.4 Theorem Classical Solutions of the PME

For some $\varepsilon > 0 \; and \; all \; x \in R^d$, let's assume that u_0 is a continuous function in R with $\varepsilon \leq u_0(x) \leq 1/\varepsilon$. Then the classical solution of the PME that exists satisfies $\varepsilon < u(x,t) < 1/\varepsilon$ for every $x \in R^d \; and \; 0 < t < \infty$. With values in the range $-1/\varepsilon \leq u_0(x) \leq -\varepsilon$, the signed PME also has classical solution and $-1/\varepsilon < u(x,t) < -\varepsilon$. when the boundary data are compatible with the initial data and satisfy the same condition $\varepsilon \leq u(x,t) \leq 1/\varepsilon \; for \; x \in \partial\Omega, t \geq 0$, a similar argument applies to the Cauchy-Dirichlet problem. The problem with zero Neuman

boundary conditions also uses the same argument. On the other hand, neither the classical theories nor the strong maximum principle can apply in the instance where the data takes zero values inside the space domain Ω, and avoiding the weak theories is not possible. In addition, phenomena like finite propagation and free boundaries appear.

2.2 Fractured Reservoirs

In geology, a fracture is the phenomenon that occurs when a stress causes a discontinuity [15] . The above definition relies more on strain effects in the Earth's crust during or after their formation. Geologists call shear fractures faults, and extension fractures joints [16]. The size of these geological features exists in a wide range, meters or kilometers in case of the longitudinal extensions, micrometers to meters in case of aperture. Moreover, several fractures or even a fracture network may be generated. For the engineers, the impact on the flow behavior of the system is very interesting. The fractures serve as a barrier blocking the flow through the surrounding matrix when the permeability in the fracture is very low. In the opposite side, for a high permeability in the fracture, the flow in the matrix is augmented by the flow in the fracture. The fracture framework is the sole contributor to the flow in case of an impermeable rock matrix or even in case of a negligible matrix permeability compared to the fracture permeability.

The representative elementary volume (REV) concept is affected by the REV size [17] because fractures are heterogeneities of the porous system according to the differentiation. The modeling of overall flow in fractured porous media becomes more complicated. Mostly, the separate treatment of the heterogeneity and the porous matrix can be used to solve this problem. We will emphasize the fracture which is filled with a porous medium on the following. In the surrounding matrix, a highly permeable fracture and less permeable porous medium characterize

the system observed. The transversal size is very small compared to the longitudinal extension of a fracture. Furthermore, the aperture is very small compared to the matrix dimensions, and its scale difference with the longitudinal widening is in orders of magnitude.

The fracture domain of a fractured system with an n-dimensional matrix domain is assumed to be an $(n-1)$-dimensional object given the above simplifications. We will use a 2-dimensional matrix domain in this study, and a 1-dimensional fracture. The fracture is treated as an interface in the matrix domain for this particular reason as shown in other works [18]. Nonetheless, even if the width of the fracture is very small, we should keep in mind that it still exists. Thus, we can only justify the reduction of the dimension if the flow velocity u_f is integrated and the pressure p_f of the fracture averaged over the width d. It is

$$u_\gamma = \int_0^d u_f \, dx_d \qquad and \qquad p_\gamma = \frac{1}{d} \int_0^d p_f \, dx_d \, , \tag{2.20}$$

where x_d is the transversal coordinate in the fracture. The consideration of an interface γ is now possible because of the mean velocity or flux u_γ and the averaged pressure p_γ. The expression of permeability coefficient with $K_\gamma = K_f d$ consolidate the resulting occurrence of the width d. The treatment of the fracture as an interface has a bearing on the velocity distribution and the pressure distribution of the fractured system. The pressure and the velocity are continuous and discontinuous respectively in case of a highly permeable fracture, which is explained by the averaging over the width of the fracture and the flow behavior of the system. The pressure is continuous as long as the fluid exhibits a tendency to flow in the fracture. Otherwise, the fluid will not enter the heterogeneity. Additionally, high flow velocities are present in the fracture. The velocities in the fracture and in the adjacent matrix should be different, and that is because of the averaging, causing a discontinuity of the velocity in the fractured system. In the opposite side, for

fractures with low permeability, that is the situation is reversed, the pressure and velocity are discontinuous and continuous respectively. Since we consider a fracture with high permeability in this endeavor, the fracture is continuous in the model concept. Also, we consider only discrete fractures and their intersections, which leads to the following cases of fractured system: a single fracture (in the vertical, the horizontal or the tilted direction), multiple intersecting fractures and a fracture which splits. More situations can be derived from these basic cases and thus are not taken into account at this point.

By the classification of fractured system [19], there are four types of fractures as described as follows (see Figure 2.1).

- Primary or Hydraulic fractures. When we are injecting the hydrofracturing fluids into formation (with or without proppants), we will generate this type of fracture. The high permeability flow paths that allow fluid to flow easily from the formation matrix into the well is provided by proppants.
- Secondary fractures. We call this type of fractures secondary because they are created as consequences from the change of geomechanical status of a rock when hydraulic fractures are being created.
- Natural fractures. These are the fractures that naturally exists in the reservoir.
- Radial fractures. These are generated by the stress in the neighborhood of the horizontal well.

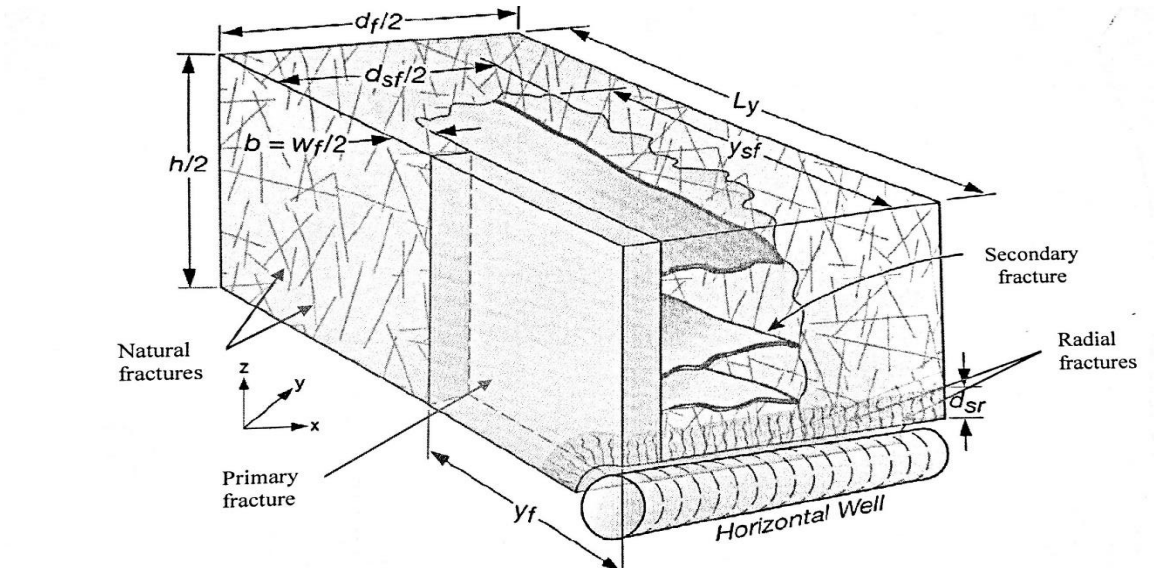

Figure 2.1 Types of fractures [20].

Since secondary fracture is generated as a consequence from primary fracture, and there are two possible fracture geometries network [21].

- Regular or ideal fractures. The planner and orthogonal is called regular or ideal fracture. Figure 2.2(A) gives an illustration of this fracture geometry.
- Irregular or non-ideal fractures. We can see these types of fractures in our life. The fractures that intersect either the well (for primary fracture) or primary fractures (for secondary

fractures) at angles other than 90 are called non-orthogonal. Also, they could be non-planner as illustrated in Figures 2.2(B) and 2.2(C).

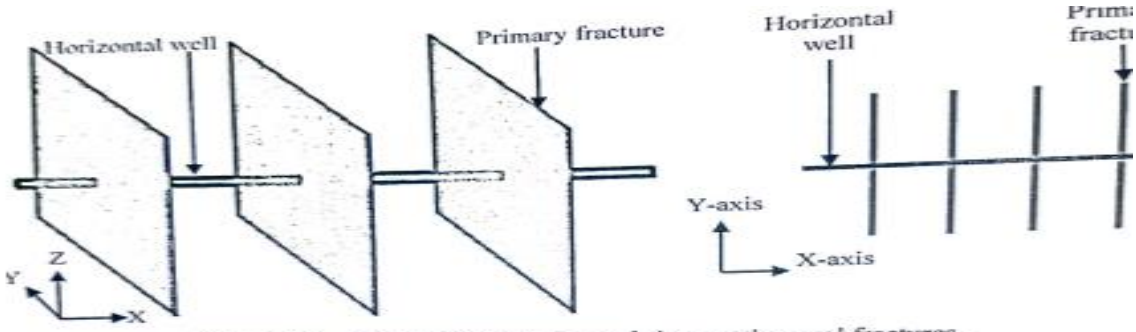

Figure 2.2A—3D and 2D plan views of planar orthogonal fractures.

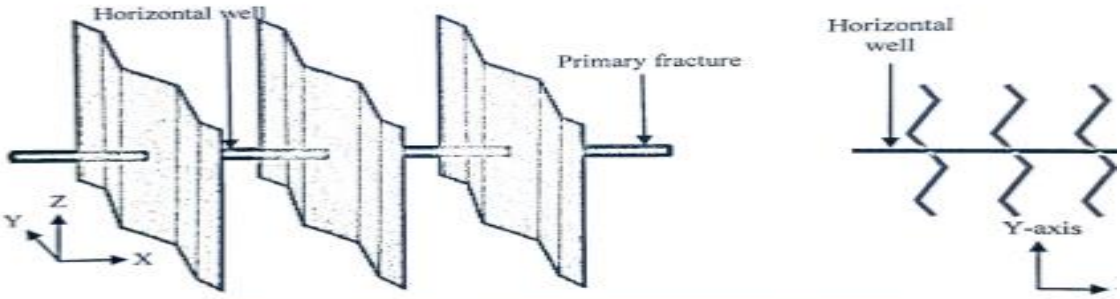

Figure 2.2B—3D and 2D plan views of non-planar fractures.

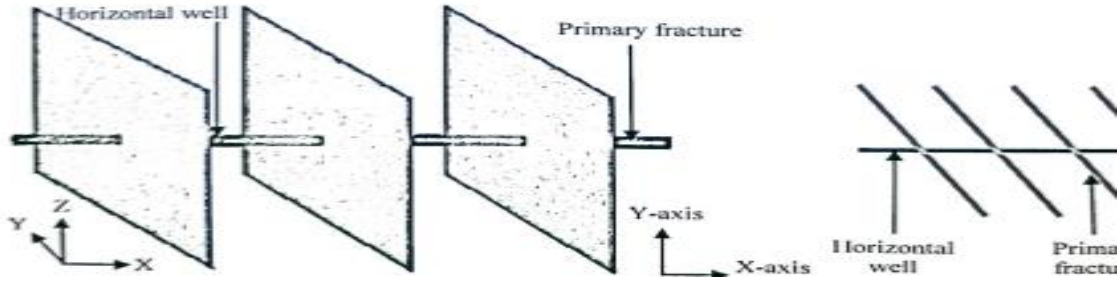

- Figure 2. 2 Classefication depends on the geometry network between two fractures [20].

2.2.1 Pseudo Steady State Models

An analysis based on sugar cube idealization of the fractured reservoir (see Figure 2.3) was conducted by Warren & Root in 1963, in which the flow between the matrix and fracture system was assumed to be in pseudo-steady state. In other words, at initial time, the pressure at the middle

of the matrix block starts. They solved simultaneously at a mathematical point a differential form for the matrix and another one for fracture. The fracture-matrix interaction is related by:

$$\boldsymbol{q = \alpha \frac{k_m}{\mu} (p_m - p_f)} \qquad \text{..... (2.21)}$$

with q being the transfer rate, μ being the fluid viscosity, α being the shape factor, k_m being the matrix permeability, and $\boldsymbol{(p_m - p_f)}$ being the pressure difference between the matrix and the fracture.

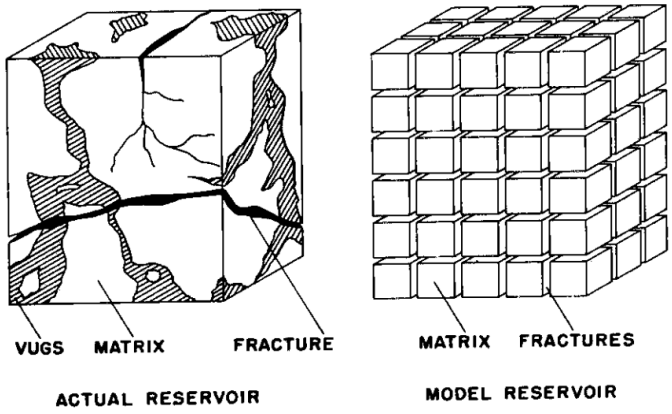

Figure 2. 3 Idealization of the heterogeneous porous medium [3].

2.2.2 Unsteady State Models

Unsteady state or transient flow conditions between matrix and fracture systems are assumed in other models (see Kazemi 1969 [22], de Swaan 1976 [23], and Ozkan. 1987 [24]). In 1969, the slab dual-porosity model (Figure 2.4) was introduced by Kazemi who also provided a numerical solution for dual-porosity reservoirs for the above case (transient). However, we should note that his solution is different than that of Warren & Root only for the transition period between the matrix and fractures systems.

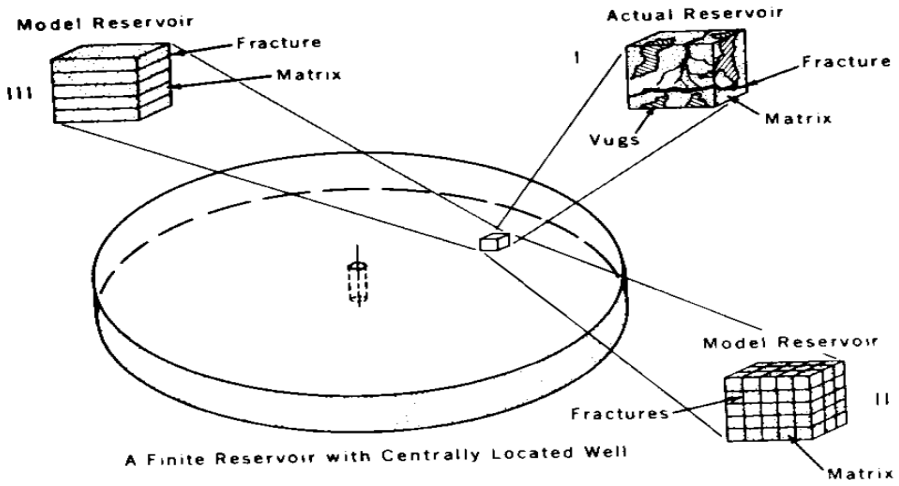

Figure 2. 4 Idealization of the heterogeneous porous medium [22].

2.2.3 Linear Flow in Fractured Reservoirs

Due to the flow and the flow surface being perpendicular, linear flow occurs at early time. In 2007 [25], different causes for linear transient flow such as high permeability layers draining adjacent tight layers, hydraulic fracture draining a square geometry, and early-time constant pressure drainage from different geometries were identified. Novel linear dual-porosity solutions were developed by El-Banbi in 1998 [26], the solutions were for fluid in linear fractured reservoirs, and they were derived in Laplace domain for several inner and outer boundary conditions. El-Banbi has also included the skin and wellbore storage effects. The fact that the reservoir functions that are derived for radial flow in linear solutions in Laplace domain and vice versa is an important progress. In 2009, Bello [27] showed that to model the horizontal well performance in tight fractured reservoir, the above solutions are introduced by El-Banbi. Next, Bello analyzed rate transient in horizontal multi-stage fractured shale gas wells by applying the constant pressure solution. Bello [28]and Bello and Wattenbarger [29], [27], [30] analyzed the shale gas wells by using the dual porosity linear flow model. They have found that among the five flow regions that

they have defined based on the linear dual-porosity constant pressure solutions, region four can effectively analyze shale gas wells performance. They have suggested that the early flow periods are affected by the skin effect, and for that they have modified an algebraic equation to account for it.

In 2009, Ozkan [31] et al and Brown et al. analyzed well tests in gas wells and proposed a tri-linear model. They have considered three contiguous media: dual-porosity inner reservoir between the hydraulic fractures, finite conductivity hydraulic fractures and outer reservoir beyond the tip of the hydraulic fractures, it was found that the outer reservoir's contribution to the flow was minimal. In 2010, Al Ahmadi [32] used the slab and cube dual-porosity idealizations to analyze shale gas wells.

CHAPTER 3

FINITE ELEMENT METHOD AND MESH ADAPTATION

This chapter gives a brief explanation about how to solve PME using finite element method with software FreeFem++. The weak formula will be derived. Also meth adaptation method is introduced.

3.1 Finite Element Method

3.1.1 Discretization with the Finite Element Method

When modeling, the model should be a close representation of the reality. However, it is difficult and sometimes even impossible to obtain the exact solution of the model. We need to numerically find a solution that is acceptable as an approximation to the physically exact solution. In mathematics terms, this means that we should find an approximated space of finite dimensions by reducing the initially infinite space of the exact solutions, this procedure is called discretization. Basically, a grid is used to discretize the domain of interest. We can use structured or unstructured grids according to our needs which are dictated by the application itself. The mesh elements are polygons in case of a 2-dimensional space. Usually convex polygons such as triangles and quadrangles are more common, and the solution is approximated on the nodes of the mesh.

The finite element (FE) method can be applied to compute approximate values of the pressure of PME at the vertices of the discretization mesh. The FE consists of two steps.

(i) We mathematically introduce the vector spaces of the function involved in the governing equations by writing the latter in variation form and multiply both sides of the equations by a test function. Then we integrate the results of this product over the domain. Since the approximated

solution is calculated globally on the whole domain, the residue exists, so comes the variation concept which can be physically explained as an attempt for global error or residual reduction.

(ii) Approximate the vector space of function to transform the above mentioned variation form into a finite dimensional system of equations. The unique values on the vertices of the mesh define a set of polynomials which represents the approximation space, meaning, two adjacent nodes of the mesh are allowed to interact by the basis function. The value of the basis function at the considered node is 1 and 0 elsewhere. Despite the functions between the nodes being continuous mostly, they can be discontinuous, they can also be of various polynomial degree all depending on how we choose the approximation space. The unknown pressure function is expanded in the discretization by the basis function.

The refinement of the mesh improves and converges the numerical solution to the analytical solution, at a condition of choosing a reasonably accurate discretization. We can compute the mean velocities of the elements using Darcy's Law starting from the numerical solution of the pressure in the last step. This method is suitable to model both the structured and unstructured grids. However, this method is not conservative because of the global integral of the differential equation. The mixed finite element method is a similar procedure that employ the local conservative mass, where we simultaneously calculate the velocities and the pressure. As can be expected, the implementation of this method is computationally expensive. The respective purpose defines which method is more suitable.

3.1.2 Linear Finite Element Formulation

In this section, we derive the linear finite element formulation of PME (2.12). Suppose that a family of simplicial meshes $\{\mathcal{T}_h\}$ is given for the physical domain Ω. We define

$$U_0 = \{v \in H^1(\Omega) | v|_{\partial\Omega} = 0\}.$$

Denote the linear finite element space associated with mesh $\mathcal{T}_h$ by U_0^h so the linear finite element solution $u^h(t) \in U_0^h$ for $t \in (0, T]$ to PME is denoted by

$$\int_\Omega \frac{\partial u^h}{\partial t} v^h \, dx + \int_\Omega K(u^h)^m (\nabla v^h)^T \nabla u^h dx = 0 \quad \forall u^h \in U_0^h, \; t \in (t_0, T] \quad (3.1)$$

Denote the number of the element, vertices, and interior vertices of $\mathcal{T}_h$ by $N, N_v and\, N_{vi}$, respectively. Assume that the first N_{vi} vertices are the interior vertices. Then U_0^h and u^h can be describe as

$$U_0^h(t) = span\{\emptyset_1, \ldots\ldots, \emptyset_{N_{vi}}\},$$

and

$$u^h = \sum_{j=1}^{N_{vi}} u_j(t)\, \emptyset_j + \sum_{j=N_{vi+1}}^{N_v} u_j(t)\, \emptyset_j \qquad (3.2)$$

where $\emptyset_j$ is the linear basis function associated with the j^{th} vertex, x_j, at the time t. The boundary and initial condition in (3.1) are approximated as

$$u_j(t) = 0, \quad j = N_{vi+1}, \ldots\ldots, N_v \qquad (3.3)$$

and

$$u_j(t_0) = u_0(x_j), \quad j = 1, \ldots\ldots, N_v \qquad (3.4)$$

Substituting (3.2) into (3.1), taking $v^h = \emptyset_i$ $(i = 1, \ldots\ldots, N_v)$, and combining the resulting equations with (3.3), we obtain the linear algebraic system

$$M \frac{du}{dt} + A(u^h)u = 0, \qquad (3.5)$$

where $\boldsymbol{u} = (\boldsymbol{u_1}, \dots\dots, \boldsymbol{u_{Nvi}}, \boldsymbol{u_{Nvi+1}}, \dots\dots, \boldsymbol{u_{Nv}})^{\boldsymbol{T}}$ is the unknown vector and *M* and *A* are the mass and stiffness matrices, respectively. The entries of the matrices are given as follows.

For $\boldsymbol{j = 1, \dots\dots, N_v}$,

$$\boldsymbol{m_{ij}} = \begin{cases} \int_{\Omega} \emptyset_j \emptyset_i \boldsymbol{dx} = \sum_{w \in \mathcal{T}_h} \int_w \emptyset_j \emptyset_i \boldsymbol{dx}, & \boldsymbol{i = 1, \dots, N_{vi}} \\ \boldsymbol{0} & \boldsymbol{i = N_{vi+1}, .., N_v} \end{cases} \tag{3.6}$$

$$\boldsymbol{a_{ij}} = \begin{cases} \int_{\Omega} \boldsymbol{K(u^h)^m (\nabla \emptyset_i)^T \nabla \emptyset_j dx} = \sum_{\boldsymbol{w \in \mathcal{T}_h}} \int_w \boldsymbol{K(u^h)^m (\nabla \emptyset_i)^T \nabla \emptyset_j dx}, & \boldsymbol{i = 1, \dots, N_{vi}} \\ \boldsymbol{\delta_{ij}} & \boldsymbol{i = N_{vi+1}, .., N_v} \end{cases}$$

3.2 Mesh Adaptation

We are going to use the free software package FreeFem++ [33] as the framework for our computations. FreeFem++ can solve partial differential equations (PDEs) using the finite element method and has built-in mesh adaptation functionality. We will apply the mesh adaptation method in FreeFem++ to solve the PME that models the fluid flow in fractured reservoir.

To determine the coordinate transformation needed for mesh generation, a functional is used in the case of variational method. The said functional usually contains a user defined monitor function and is used to estimate difficulties in the numerical approximation of the physical solution. A crucial feature in formulating the functional is the well-posedness of the functional, in other words, the existence and uniqueness of the minimizer, and the assuredness of the maximum principle. In theoretical studies, the most challenging thing to guarantee is necessary property of the non-singularity of the coordinate transformation, despite it not being a challenge numerically for systems that have a convex computational domain and satisfying the maximum principle.

Giving that the variational methods lead to nonconvex functional in two or higher dimension, scientists usually do not use standard error estimates in the development of variational methods directly. Geometric considerations are the base of developing variational methods most of the time. For example, combining mesh concentration, orthogonality and smoothness was the basis for Brackbill and Saltzman [34] to develop a famous method. the mesh adaptation functional choice for Dvinsky [35] was the energy of harmonic mappings, whereas functionals based on the idea of conditioning the Jacobian matrix of the coordinate transformation were developed by Knupp and Robidoux [36]. The behavior of the mesh for a class of functionals was quantitatively investigated by Cao et al [37]. However, it is not straightforward to choose an appropriate monitor function for some practical problems due to the lack of direct connections with error estimates in the existing method. So, more understanding of the existing methods as well as developing new methods that are error estimate oriented is needed. A criterion for mesh adaptation based on an error function was developed, the same criterion was then decomposed to the isotropy and the uniformity requirements, which are easier to work with.

Mesh adaptation is an important tool in the theorists' arsenal to use when solving differential equations and variational problems. Placing more and less mesh elements in regions of larger and less solution errors respectively, will allow for a noticeable computational efficiency. The behavior of the error in the approximation u_h dictate the generation of the mesh (Th) when our concern is the adaptive finite element solution. The last decade have witnessed the development of several algorithms and codes that deals with generating the M-uniform meshes by feeding them a metric tensor M. such algorithms are represented by advancing front method [38], the bubble mesh method [39], Delaunay-type triangulation method [40] [41] [42] [43], the method combining local modification with smoothing or node movement [44] [45] [46] [47] [48]. Hecht

also developed a code called BAMG (Bidimensional Anisotropic Mesh Generator). To specify the tensor M, other approaches have been introduced. In particular, the formulas are motivated by the work of D'Azevedo and Simpson [49] on linear interpolation for quadratic functions on triangles. In the work of reference [50], the interpolation error on simplicial elements is the base for the derivation of various metric tensor formulas. [51] [52] show that when we take the reference element $\widehat{\boldsymbol{K}}$ to be equilateral and unitary in volume, a simplicial *M*-uniform mesh $\boldsymbol{\mathcal{T}_h}$ for a given metric tensor *M =M(x)* satisfies.

$$\boldsymbol{\rho_K}|\boldsymbol{K}| = \frac{\boldsymbol{\sigma_h}}{\boldsymbol{N}} \qquad \boldsymbol{for\ all\ K} \in \boldsymbol{\mathcal{T}_h},$$

and

$$\frac{\mathbf{1}}{\boldsymbol{d}}\boldsymbol{tr}((\boldsymbol{F'_K})^{\boldsymbol{T}}\boldsymbol{M_K}\boldsymbol{F'_K}) = \mathbf{det}((\boldsymbol{F'_K})^{\boldsymbol{T}}\boldsymbol{M_K}\boldsymbol{F'_K})^{\frac{\mathbf{1}}{\boldsymbol{d}}} \qquad \boldsymbol{for\ all\ K} \in \boldsymbol{\mathcal{T}_h}.$$

With *N* representing the number of mesh elements, |K| the volume of the element K, $\boldsymbol{F_K}$ the affine mapping from $\widehat{\boldsymbol{K}}$ to K, $\boldsymbol{F'_K}$ the Jacobian matrix of $\boldsymbol{F_K}$,

$$\boldsymbol{M_K} = \frac{\mathbf{1}}{|\boldsymbol{K}|}\int_{\boldsymbol{K}} \boldsymbol{M}(\boldsymbol{x})\boldsymbol{dx}, \qquad \boldsymbol{\rho_K} = \sqrt{\mathbf{det}(\boldsymbol{M_K})}, \qquad \boldsymbol{\sigma_h} = \sum_{\boldsymbol{K}\in\boldsymbol{\mathcal{T}_h}} \boldsymbol{\rho_K}|\boldsymbol{K}|.$$

The size of K from $\boldsymbol{\rho_K}$ is determine by the equidistribution condition. The relationship between $\boldsymbol{\rho_K}$ and |K| is inversely proportional. The shape and orientation of K is characterized by the alignment condition, the principal axes of the circumscribed ellipsoid of K are parallel to the eigenvectors of $\boldsymbol{M_K}$ and their lengths to the square roots of the respective eigenvalues are reciprocally proportional.

3.3 Criteria for Mesh Adaptation

An error function was used to develop criteria for which are used to construct mesh adaptation. The said error function is distinguished from error estimates because it describes the local behavior of the error as oppose to providing its magnitude. Let $\boldsymbol{\Omega}$ and $\boldsymbol{\Omega}_{\boldsymbol{c}}$ be the physical and computational domains $\boldsymbol{in}\ \boldsymbol{\Re^n}$; $\boldsymbol{n = 1, 2\ or\ 3}$, respectively, and denote the coordinate for them by *x* and $\boldsymbol{\xi}$ for a given $\boldsymbol{u = u(x)}$. The objective is to look for a coordinate transformation $\boldsymbol{x = x(\xi)}$: $\boldsymbol{\Omega_c \longrightarrow \Omega}$ in a way that $(\boldsymbol{\hat{u}(\xi) = u(x(\xi))})$ is easier to approximate. The linear element or the function variation over differential segment $\boldsymbol{d\xi}$ in $\boldsymbol{\Omega_c}$ are considered, with the Jacobian matrix of the coordinate transformation being denoted by $\boldsymbol{J = \partial x / \partial \xi}$. We should also chose $\boldsymbol{x = x(\xi)}$ in a way that $\boldsymbol{J^T[I + \nabla u \nabla u^T]J = cI}$, with *I* representing the identity matrix and c being a constant. In this way, we can resolve $\boldsymbol{\hat{u}}$ on a computational mesh because it has a constant variation, the mesh is usually chosen to be regular and uniform. The interpolation error estimates are an additional motivation for easy numerical approximation. Denote the linear interpolant of u at the vertices of a two-dimensional triangle imaging mesh cell as $\boldsymbol{\prod_1 u}$ and denote the error as $\boldsymbol{E_0(x) = \prod_1 u - u}$. We can then express $\boldsymbol{E_0}$ locally as a quadratic function, and we can also express its level surfaces from a family of ellipses with a shared center x_c, given that the Hessian matrix (H) of u is positive definite. Geometrically, the circum-surface of the cell that belongs to the above group of ellipses is the level surface of value zero.

For x close to x_c, Dzevedo [53] has shown that it is possible to write $\boldsymbol{E_0}$ as

$$\boldsymbol{E_0(x) \approx E_0(x_c) - \frac{1}{2} dx^T H dx},$$

where dx = x-x_c, and the Hassian matrix H is computed at x = x_c. In addition, it was proven by Dzevedo and Simpson [49] that the gradient of the linear interpolation error is given by

$$\boldsymbol{E_G(x) = \left\| \nabla u - \prod\nolimits_1 u \right\|_{l^2} \approx \sqrt{dx^T H^T H dx}}.$$

Writing $\boldsymbol{dx = J d\xi}$, we have $\boldsymbol{E_0(x) \approx E_0(x_c) - \frac{1}{2} d\xi^T J^T H J d\xi}$ or $\boldsymbol{E_G(x) \approx \sqrt{d\xi^T J^T H^T H J d\xi}}$.

Once again, a good choice for the coordinate transformation when trying to resolve u using a linear interpolation on a regular and uniform mesh is $\boldsymbol{J^T H J = cI}$ or $\boldsymbol{J^T H^T H J = cI}$ for some constant c. It only makes sense to suggest that some error estimates can be characterized by a quadratic function given the above formula for the solution variation and linear interpolation error estimates. A general error function is defined for that particular reason as $\boldsymbol{E(x) = \sqrt{d\xi^T J^T G J d\xi}}$ with ξc is an arbitrary point in $\boldsymbol{\Omega_c}$; $\boldsymbol{d\xi = \xi - \xi_c}$, and *G=G(x)* is an n-by-n matrix defined by the user that represent the monitor function, the matrix is symmetric and positive definite. To avoid any confusion, we adopt the following assumption: coordinate x and ξ in the above equation are related by the coordinate transformation $\boldsymbol{x = x(\xi)}$ and $\boldsymbol{J^T G J}$ is computed at $\boldsymbol{\xi_c}$ and the task now is to derive $\boldsymbol{x = x(\xi)}$ such that for a given positive constant c, $\boldsymbol{J^T G J = \frac{1}{c} I}$ or $\boldsymbol{J^{-1} G^{-1} J^{-T} = cI.}$

The above equation is unfortunately not practical to obtain. Rewrite it as $\boldsymbol{(J^{-1}M^{-1})(J^{-1}M^{-1})^T = cI,}$ it is straightforward to show that $\boldsymbol{J^{-1}M^{-1} = \sqrt{c}\, Q}$ for an arbitrary orthogonal matrix Q. The last equation implies that in case of no adaptation (G=*I*), the coordinate transformation is orthogonal irrespective of the physical and computational domain, which is of course impossible. We then introduce two relatively easier conditions to develop functionals that fulfill this criterion. The above equation is similar to requiring that the determinant of $\boldsymbol{A \equiv J^{-1} G^{-1} J^{-T}}$ is constant and the eigenvalues are equal. An isotropic and uniform distribution are forced on to the error function

E(x) by the last two conditions. For further elucidation, using the eigen-decomposition $\boldsymbol{A} = \boldsymbol{UDU^T}$, given that $\boldsymbol{D} = \boldsymbol{diag}(\boldsymbol{\lambda_1}, \ldots\ldots, \boldsymbol{\lambda_n})$ and U is an orthogonal matrix, we achieve the level surface as

$$(\boldsymbol{\xi} - \boldsymbol{\xi_c})^T \boldsymbol{UD^{-1}U^T}(\boldsymbol{\xi} - \boldsymbol{\xi_c}) = \boldsymbol{e^2} \text{ or } \sum_{\boldsymbol{i}} \left(\frac{\tilde{\boldsymbol{\xi}}^{\boldsymbol{i}} - \tilde{\boldsymbol{\xi}}_{\boldsymbol{c}}^{\boldsymbol{i}}}{\sqrt{\boldsymbol{\lambda_i}}} \right) = \boldsymbol{e^2}$$

with e is a given error cutoff, and $\tilde{\boldsymbol{\xi}} - \boldsymbol{\xi_c} = \boldsymbol{U^T}(\boldsymbol{\xi} - \boldsymbol{\xi_c})$. According to the isotropy condition, the above ellipse is similar to a sphere, in the other hand, the associated ellipsoid should have a constant volume with respect to location in $\boldsymbol{\Omega_c}$ which is implied by the uniformity requirement.

We use the software FreeFem ++, where the metric tensor for mesh adaptation depends on the Hessian $(\mathcal{H})\ D^2 f = \begin{bmatrix} \frac{\partial^2 f}{\partial x^2} & \frac{\partial^2 f}{\partial x \partial y} \\ \frac{\partial^2 f}{\partial x \partial y} & \frac{\partial^2 f}{\partial y^2} \end{bmatrix}$, to generate new mesh. By the equi-distribution of errors we compute our metric tensor $\mathcal{M}$ as follows.

$$\mathcal{M} = \left(\frac{1}{err\ coef^2} \frac{|\mathcal{H}|}{\sup(\eta) - \inf(\eta)} \right)^p.$$

CHAPTER 4

NUMERICAL RESULTS

In this chapter, we will present numerical results for this type of PME.

$$\partial_t u = \nabla.(K u^m \nabla u) \qquad (4.1)$$

We use FreeFem++ software to solve this PME by finite element method and compare the results with and without adaptation to show the advantages of mesh adaptation. We present the results for one-dimensional and two-dimensional problems.

4.1 One Dimension (1D)

We solve this equation in 1D because we would like to compare our adaptive meshes with log-spacing meshes that are commonly used by other researchers. Also, log-spacing method works for 1D meshes and complicated treatment is needed to apply it for 2D meshes. We divide the results into two parts: without adaptation and with adaptation.

4.1.1 Without Adaptation

We solve (4.1) using uniform meshes without fracture and uniform mesh with fracture.

4.1.1.1 Example 1. For this example, we consider uniform mesh without fracture. We will solve (4.1) with

$$\beta = \frac{1}{2m+2} \quad and \quad t_o = \frac{1}{2}\beta m {r_0}^2 \qquad dt = \frac{t_f - t_0}{n_t}$$

$$u_0(x) = \begin{cases} \left(1 - \frac{(x-0.5)^2}{r^2}\right)^{\frac{1}{m}} & if\,|x-0.5| < r \\ 0 & otherwise \end{cases}$$

Where m is the ratio of heat capacity, radius of initial support is r=0.2 and $t_o$is the initial time, $t_f = 0.05$ and $n_t = 50$. Our domain for this example is $\Omega = [0,1]$ and the permeability K=1 for the whole domain and we divide our domain to $n_x = 40$ subintervals. We solve it for m=1, m=2 and m=5.

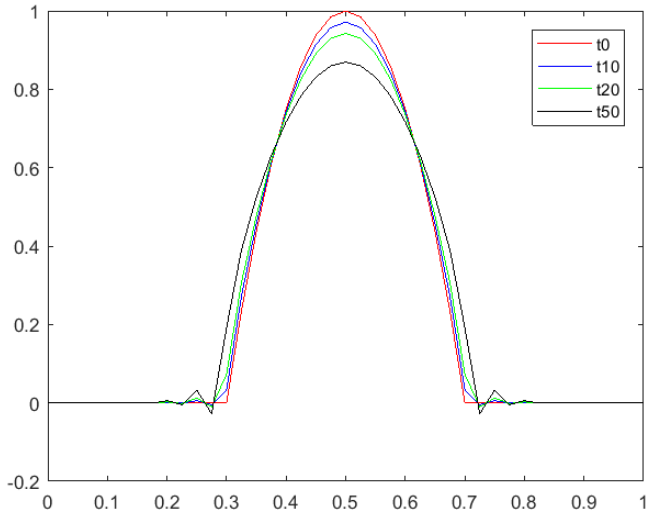

Figure 4.1 No fracture without adaptation, m=1.

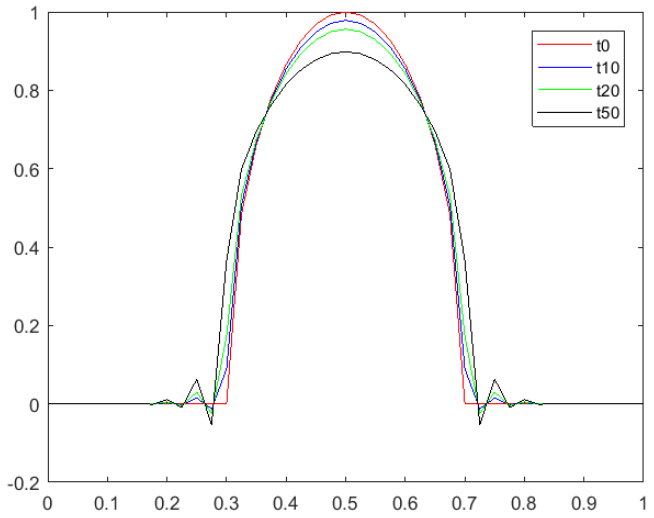

Figure 4.2 No fracture without adaptation, m=2.

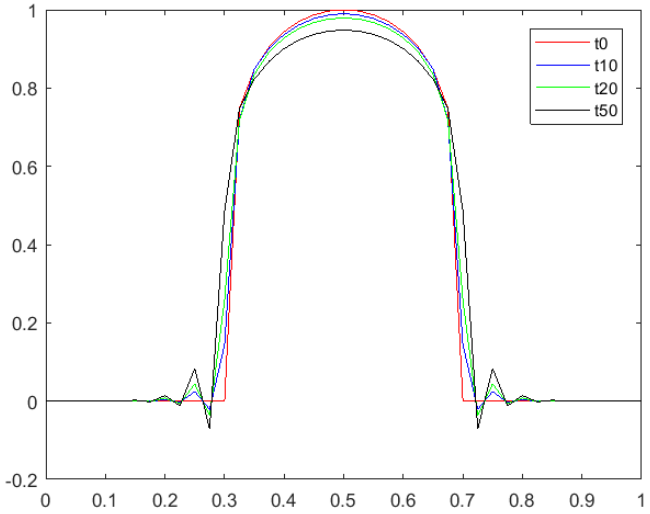

Figure 4.3 No fracture without adaptation, m=5.

In Example 1, the algorithm for our code generates uniform meshes by dividing interval (0,1) on x-axis into $n_x = 40$ subintervals. We plot the results when $n_t = 0,10,20\ and\ 50$ such that t=0.006, 0.008, 0.0106 and 0.05, respectively. In Figure 4.1 at t_0 is the initial solution and u=1 when x=0.5. When the time changes, we see the final solution at t_{50} is $u \approx 0.8$ for m=1, $u \approx 0.85$ at m=2 in Figure 4.2 and $u \approx 0.9$ at m=5 in Figure 4.3. We can observe that the positive solutions propagate outwards and the values become smaller. For different values of m, when m is larger, the solution propagates slower.

4.1.1.2 Example 2. For this example, we consider uniform mesh with a fracture in the center of the domain. The difference from the Example 1 is in *K* such that

$$K = \begin{cases} 10^4 & 0.48 \le x \le 0.52 \\ 1 & otherwise \end{cases}$$

And $t_0, u_0,\ n_t, t_f, n_x$ will be the same as those in Example 1. We also solve (4.1) for *m=1*, *m=2* and *m=5*. $K=10^4$ in the center is much larger than *K=1* at other places indicates the existence of a fracture.

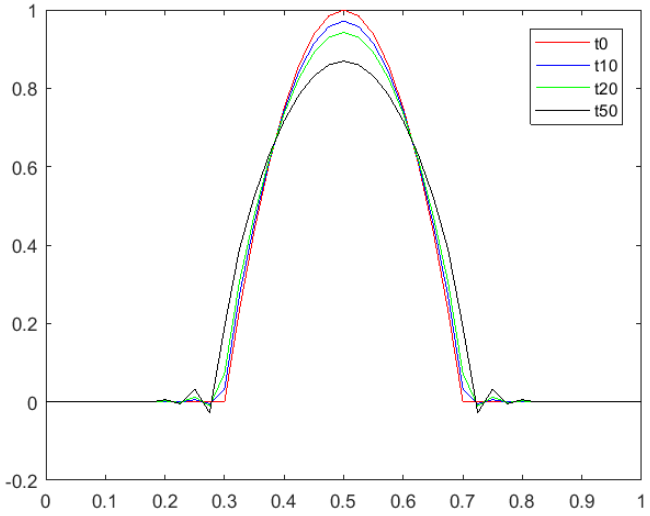

Figure 4.4 Fracture without adaptation, m=1.

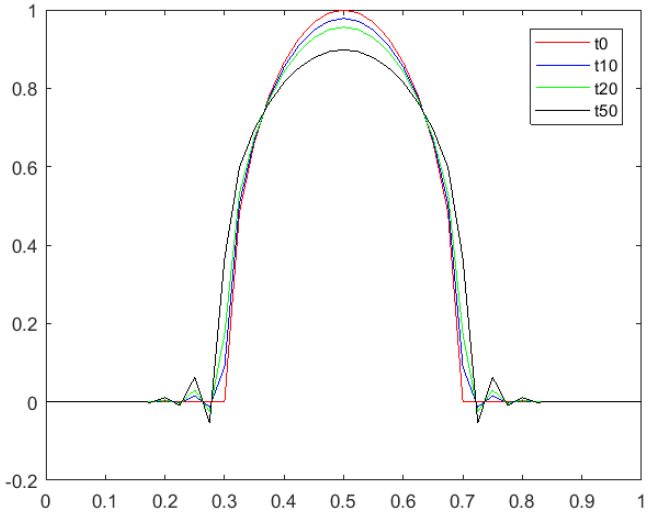

Figure 4.5 Fracture without adaptation, m=2.

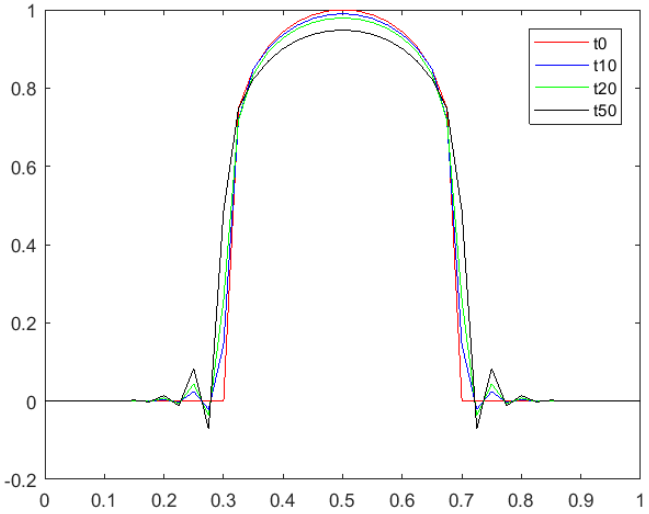

Figure 4.6 Fracture without adaptation, m=5.

In Example 2, we observe that the solutions are still higher than 0.8 in the center (see Figures 4.4, 4.5, 4.6) from x=0.3 to x=0.7.

4.1.2 With Adaptation

In this part we consider log-spacing mesh without fracture, log-spacing mesh with fracture, uniform mesh without fracture and uniform mesh with fracture.

4.1.2.1 Example 3. In this example we consider log-spacing without fracture. Log-spacing method means $|lnx_n - lnx_{n-1}| = |lnx_{n-1} - lnx_{n-2}|$. We will use the same parameters as in Example1.

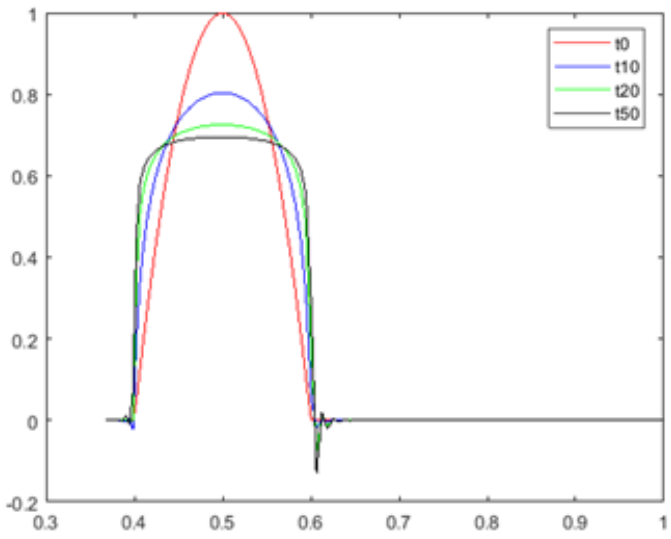

Figure 4.7 Log-spacing without fracture, m=1.

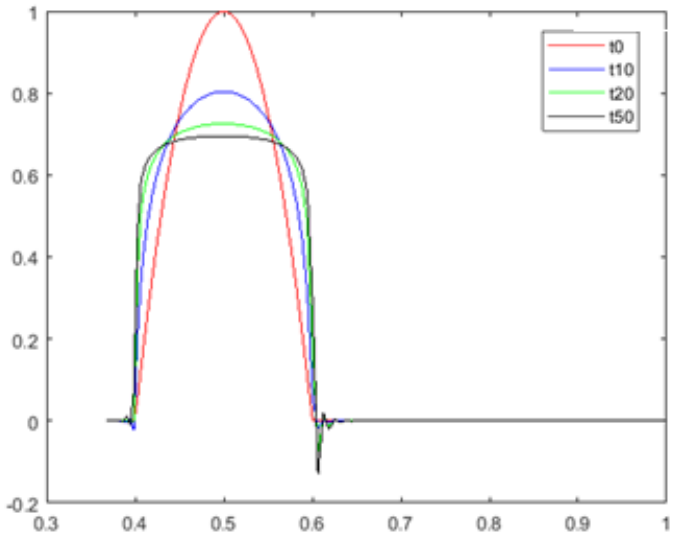

Figure 4.8 Log-spacing without fracture, m=2.

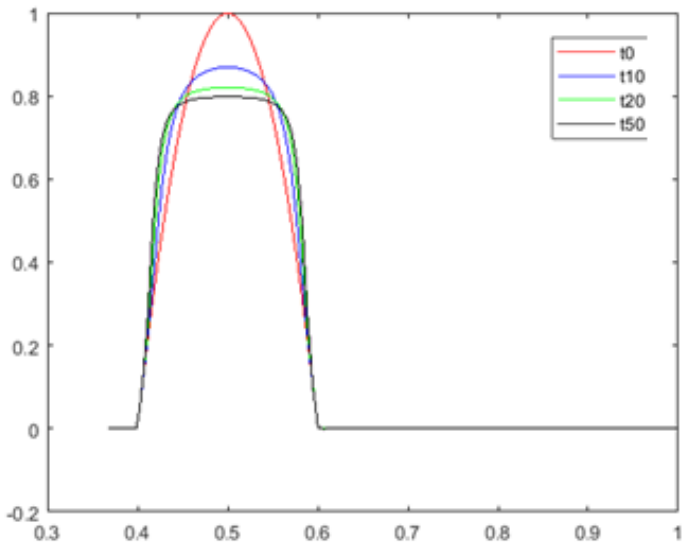

Figure 4.9 Log-spacing without fracture, m=5.

In Example 3, we divide the interval as $(e^{-40}, e^{-39}, \ldots\ldots, e^{0} = 1)$. At t_0, the initial solution is still the same but at t_{50} the final solution is different such as $u_{50} \approx 0.6$ in Figure 4.7 for m=1, $u_{50} \approx 0.65$ in Figure 4.8 for m=2 and $u_{50} \approx 0.78$ in Figure 4.9 for m=5.

The propagation of the positive solution seems confined by the initial compact support, which is not reasonable. There may exist some mistakes in the computing codes and more investigation is needed to address this issue.

4.1.2.2 Example 4. In this example we consider log-spacing with fracture. We will use the same parameters as in Example 2.

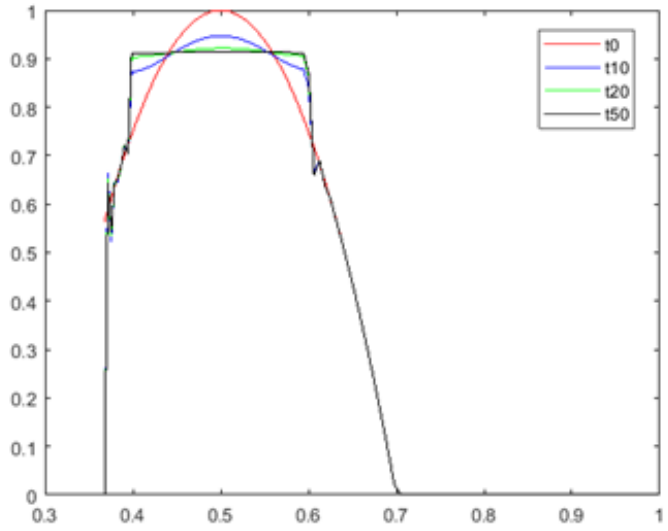

Figure 4.10 Log-spacing with fracture, m=1.

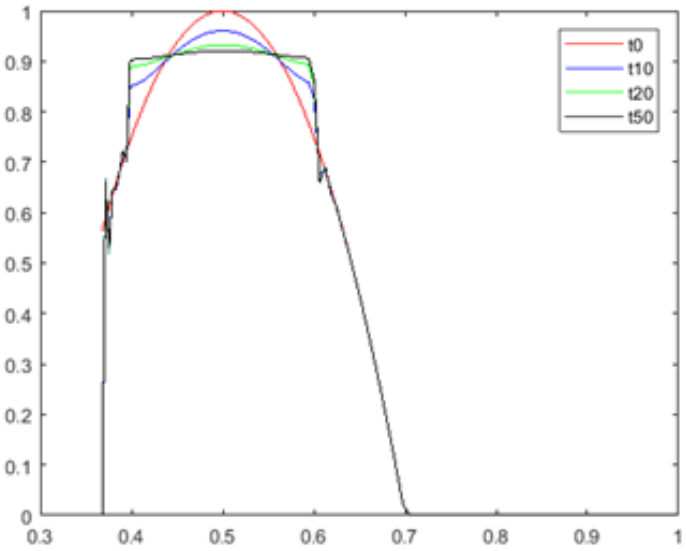

Figure 4.11 Log-spacing with fracture, m=2.

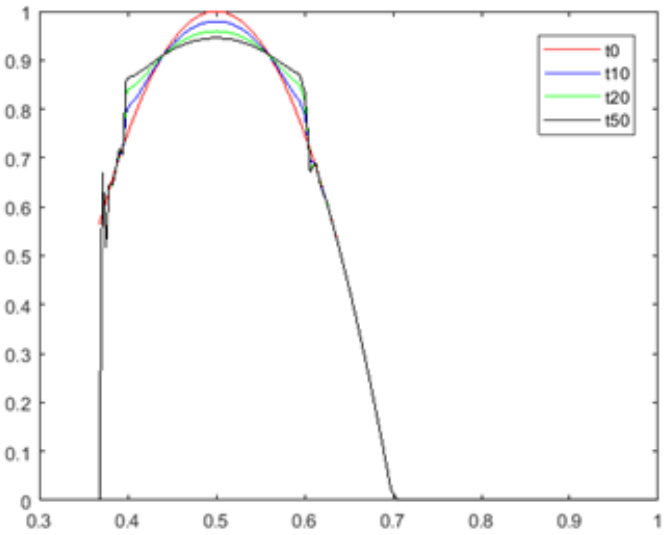

Figure 4.12 Log-spacing with fracture, m=5.

In Example 4, the numerical solution looks unreasonable and more investigation is needed to address the issue.

4.1.2.3 Example 5. In this example we consider uniform mesh without fracture and we will adapt the initial mesh and solve it again with adaptive mesh. We will use the same parameters as in Example 1.

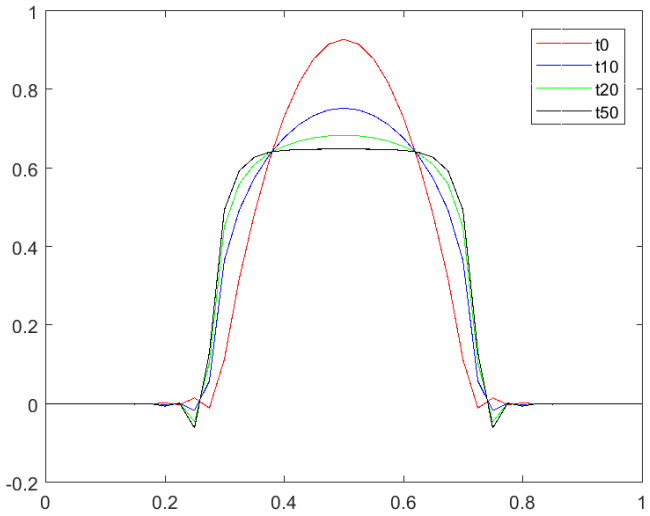

Figure 4.13 Adaptation without fracture, m=1.

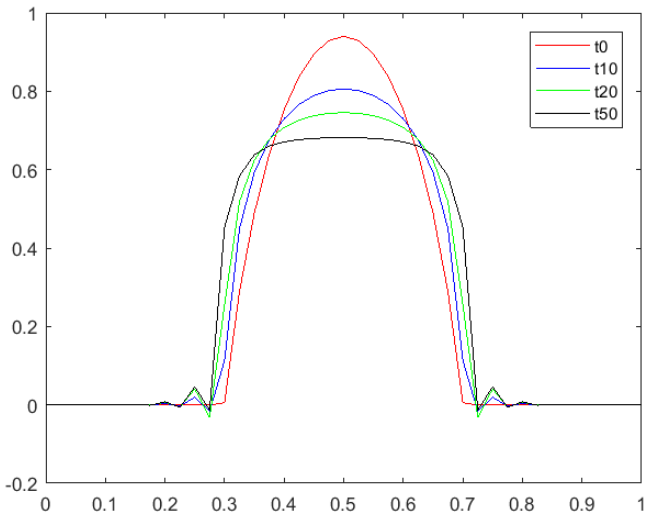

Figure 4.14 Adaptation without fracture, m=2.

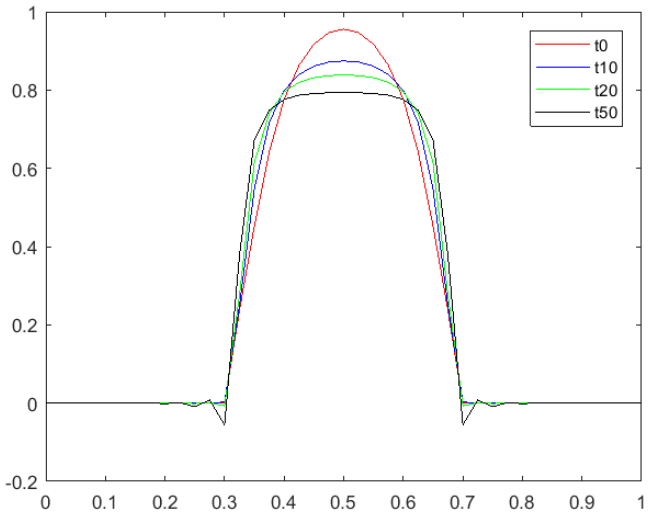

Figure 4.15 Adaptation without fracture, m=5.

At first, we generate the same uniform mesh as in Example 1. Then we compute the solution on the uniform mesh. After that we compute the metric tensor M based on the solution on uniform mesh and adapt the mesh according to the metric tensor. Finally, we compute the solution on the new adaptive mesh.

In Example 5, we see the final solution is very close to the exact solution. For example, in Figure 4.13, the final solution at t_{50} is $u_{50} \approx 0.6$ for m=1, $u_{50} \approx 0.63$ for m=2 in Figure 4.14, and $u_{50} \approx 0.78$ for m=5 in Figure 4.15. The results show that adaptive mesh provides better results than uniform mesh and log-spacing mesh.

4.1.2.4 Example 6. In this example we consider uniform mesh with fracture and we will adapt the initial mesh and solve it again with adapt mesh. We will use the same details as in Example 2.

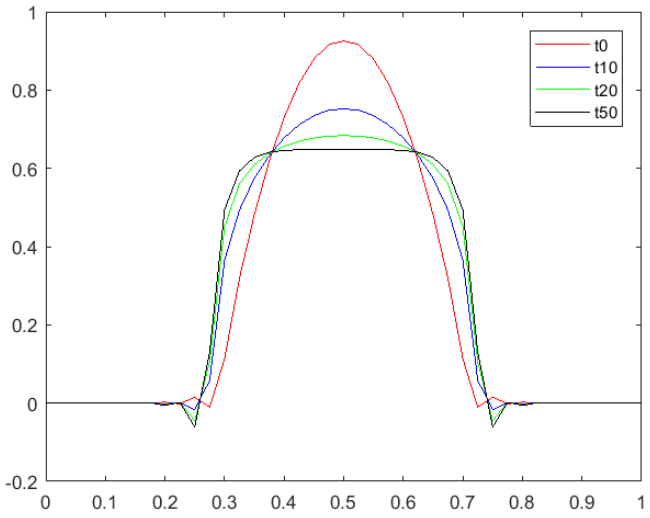

Figure 4.16 Adaptation with fracture, m=1.

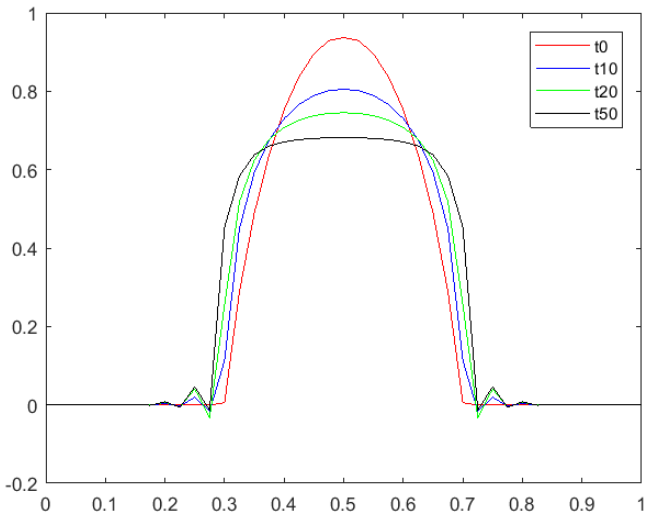

Figure 4.17 Adaptation with fracture, m=2.

No table of figures entries found.

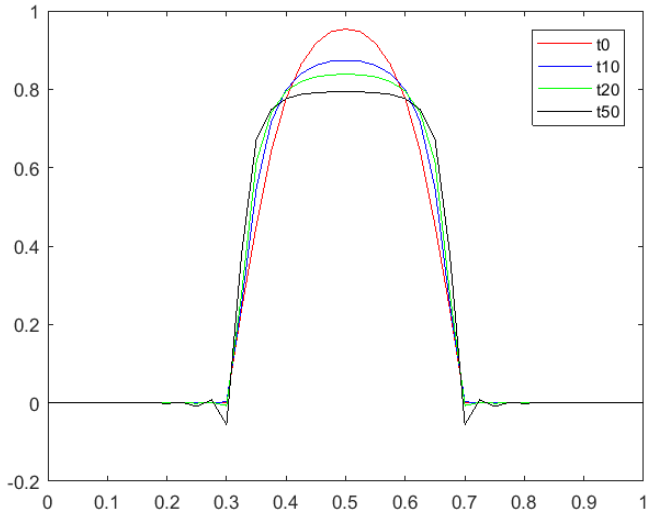

Figure 4.18 Adaptation with fracture, m=5.

In Example 6, we see the final solution is also close to the exact solution. In Figure 4.16, the final solution at t_{50} is $u_{50} \approx 0.6$ for m=1, $u_{50} \approx 0.63$ for m=2 in Figure 4.17, and $u_{50} \approx 0.78$ for m=5 in Figure 4.18.

4.1.3 Error in 1D

After the above numerical results for uniform mesh, log-spacing mesh and adaptive mesh, we compute the L^2-norm of error for the numerical solutions at t_f to see the convergence of the approximation errors. The exact solution is $u_{exact} = \max\begin{cases}\frac{1}{k}(1-\frac{(x-0.5)^2}{k^2r^2})^{\frac{1}{m}} \\ 0\end{cases}$ where $k = {t_f}/{t_0}$ and the averaged L^2-norm of error is

$$Error = \frac{\sqrt{\int (u-u_{exact})^2 dx}}{N_e} \qquad where\ N_e\ is\ the\ number\ of\ element.$$

Table 4.1. L^2-norm of error for numerical solutions using different meshes

N_e	10	20	40	60	100	160
Uniform mesh	3×10^{-2}	1×10^{-2}	8×10^{-3}	5×10^{-3}	3×10^{-3}	2×10^{-3}
Log-spacing	1×10^{-2}	5×10^{-3}	3×10^{-3}	2×10^{-3}	1×10^{-3}	7×10^{-4}
Adaptation	5×10^{-3}	8×10^{-4}	5×10^{-4}	4×10^{-4}	3×10^{-4}	2×10^{-4}

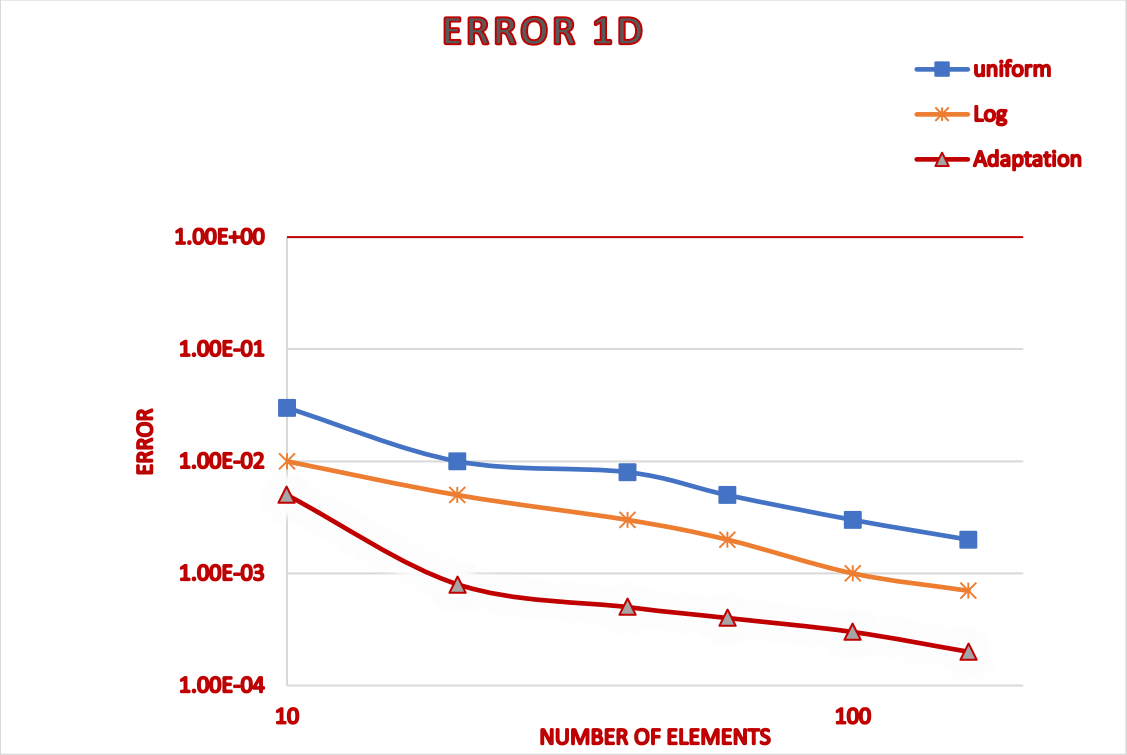

Figure 4.19 L^2-norm of error in log-log scale.

As we see in this Table 4.1 and in Figure 4.19, the error for uniform mesh is the highest and the error for adaptive mesh is the lowest. Also, the error with adaptive mesh decreases faster than other meshes.

4.2 Two Dimension (2D)

In this section, we presents the results for 2D meshes.

4.2.1 Without Adaptation

We solve (4.1) using uniform mesh without fracture and uniform mesh with fracture.

4.2.1.1 Example 7. For this example, we consider uniform mesh without fracture. We will solve (4.1) with

$$\boldsymbol{\beta} = \frac{\mathbf{1}}{\mathbf{2m+2}} \qquad \boldsymbol{and} \qquad \boldsymbol{t_o} = \frac{\mathbf{1}}{\mathbf{2}}\boldsymbol{\beta m r_0}^{\mathbf{2}} \qquad \boldsymbol{dt} = \frac{\boldsymbol{t_f - t_0}}{\boldsymbol{n_t}}$$

$$\boldsymbol{u_0(x)} = \begin{cases} \left(1 - \dfrac{(\boldsymbol{x-0.5})^{\mathbf{2}} + (\boldsymbol{y-0.5})^{\mathbf{2}}}{\boldsymbol{r^2}}\right)^{\frac{1}{m}} & \boldsymbol{if}\ (\boldsymbol{x-0.5})^{\mathbf{2}} + (\boldsymbol{y-0.5})^{\mathbf{2}} < \boldsymbol{r^2} \\ \mathbf{0} & \boldsymbol{otherwise} \end{cases}$$

where m is the ratio of heat capacity, radius of initial support is r=0.2 and t_o is the initial time, $t_f = 0.01$ and $n_t = 10$. Our domain for this example is $\Omega = [0,1]^2$ and the permeability K=1 for the whole domain. We solve it for m=1, m=2 and m=5.

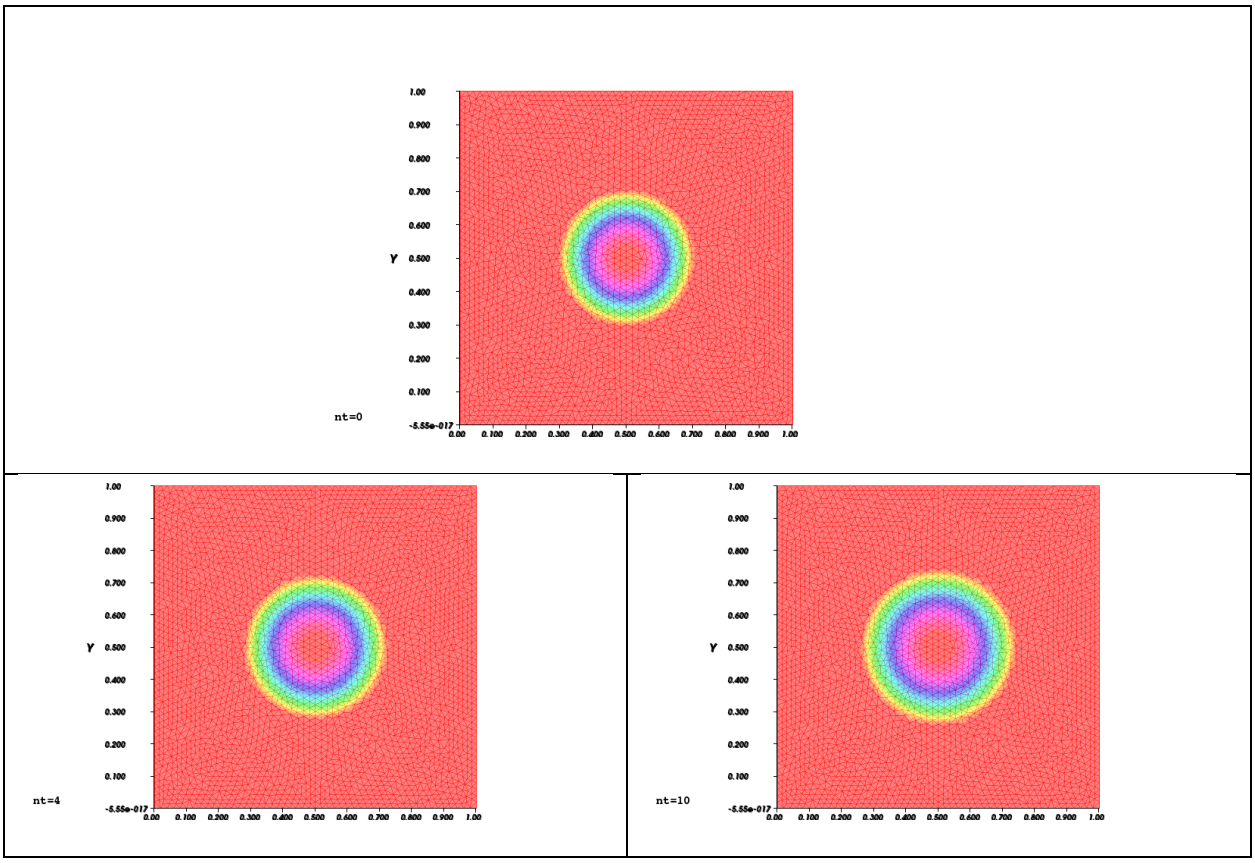

Figure 4.20 2D, no fracture, no Adaptation, m=1.

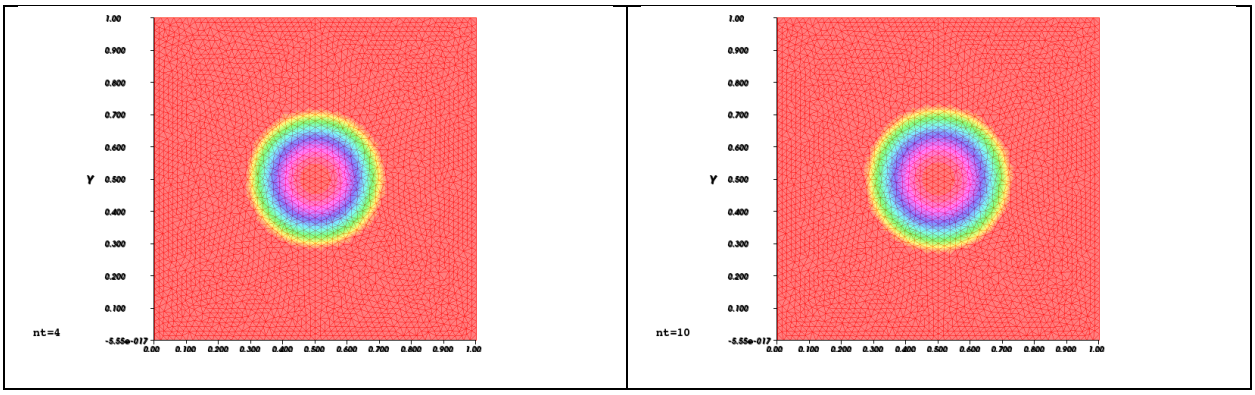

Figure 4.21 2D, no fracture, no Adaptation, m=2.

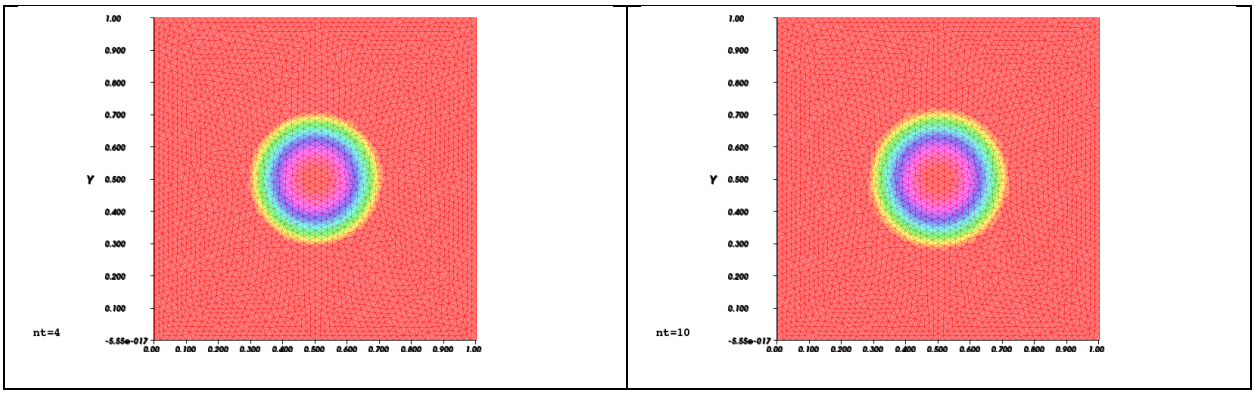

Figure 4.22 2D, no fracture, no adaptation, m=5.

In Example 7, we can see the solution distribution in the reservoir, and the support becomes larger when time changes which indicates the propagation is in outwards direction. Also, the propagation is slower when m increases as can be seen in Figures 4.20, 4.21, and 4.22.

4.2.1.2 Example 8. In this example, we consider uniform mesh with a fracture in the center of x-direction. The difference from the Example 1 is *K* such that

$$K = \begin{cases} 10^4 & inside\ the\ fracture \\ 1 & otherwise \end{cases}$$

And $t_o, u_0,\ n_t, t_f$ are the same as in Example 7. We put three fractures ($n_f = 3$) with width of fracture ($w_f = 0.02$) and height of fracture ($h_f = 0.4$). Also, we solve (4.1) for m=1, m=2 and m=5.

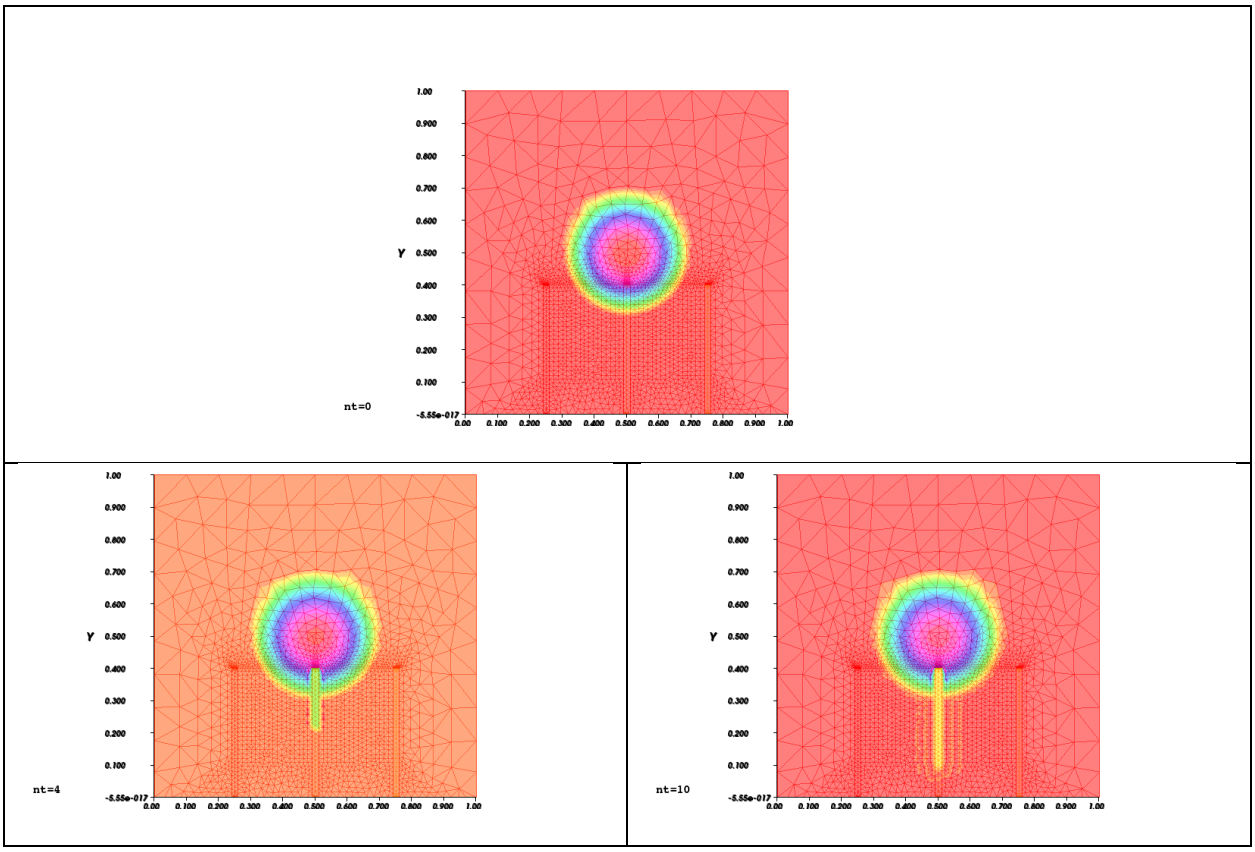

Figure 4.23 No adaptation with fracture, m=1.

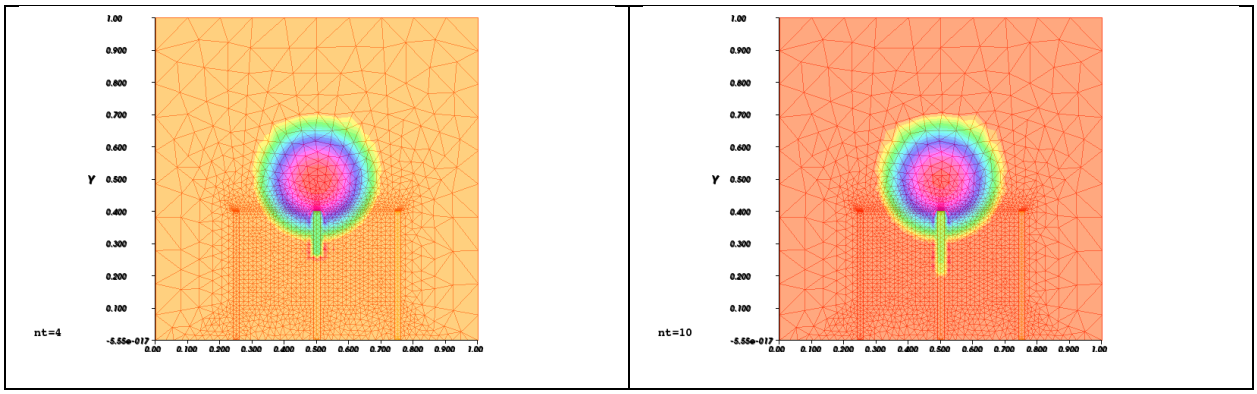

Figure 4.24 No adaptation with fracture, m=2.

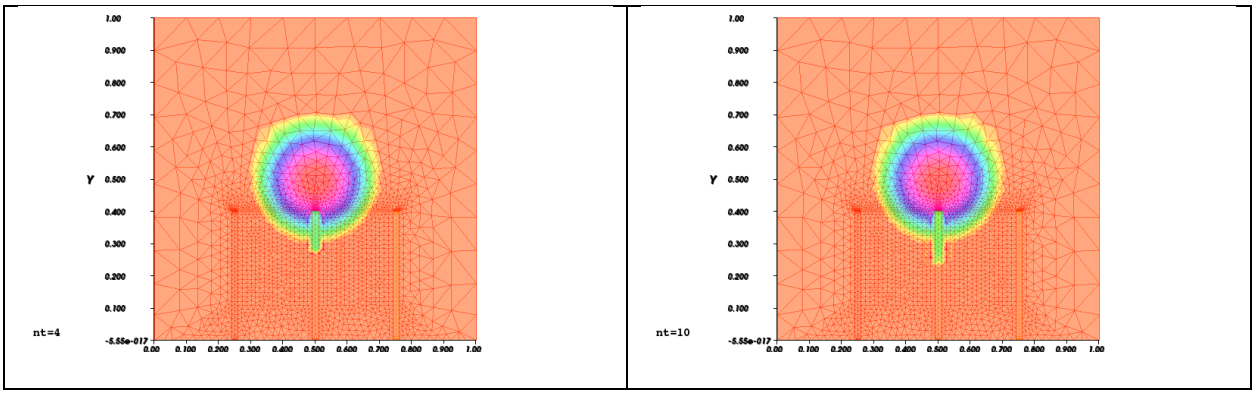

Figure 4.25 No adaptation with fracture, m=5.

In Example 8, the initial solution is still the same as in Example 7. The observation is consistent with those in 1D. For m=1 in Figure 4.23 at $n_t = 4$, the solution inside the fracture is around 0.25 and at $n_t = 10$ the boundary of the support almost reaches the horizontal well. Also, for m=2 in Figure 4.24 at $n_t = 10$, the solution value is smaller than for m=1 and higher than for m=5 in Figure 4.25. The propagation is slower when m is larger. For m=5, the boundary of the support even has not reached the fractures at $n_t = 4$.

4.2.2 With Adaptation

4.2.2.1 Example 9. In this example we consider uniform mesh without fracture and we will adapt the initial mesh and solve it again with adaptive mesh. We will use the same parameters as in Example 7.

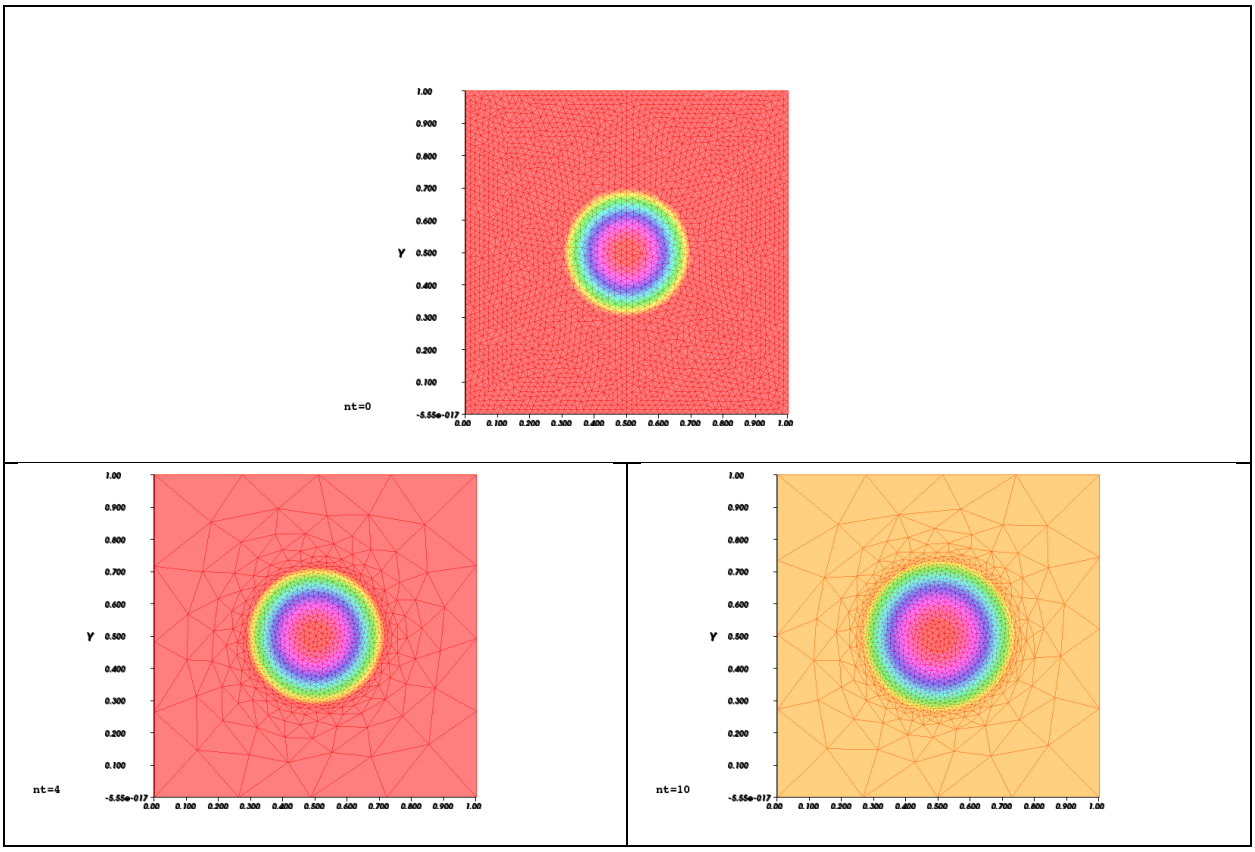

Figure 4.26 No fracture with adaptation, m=1.

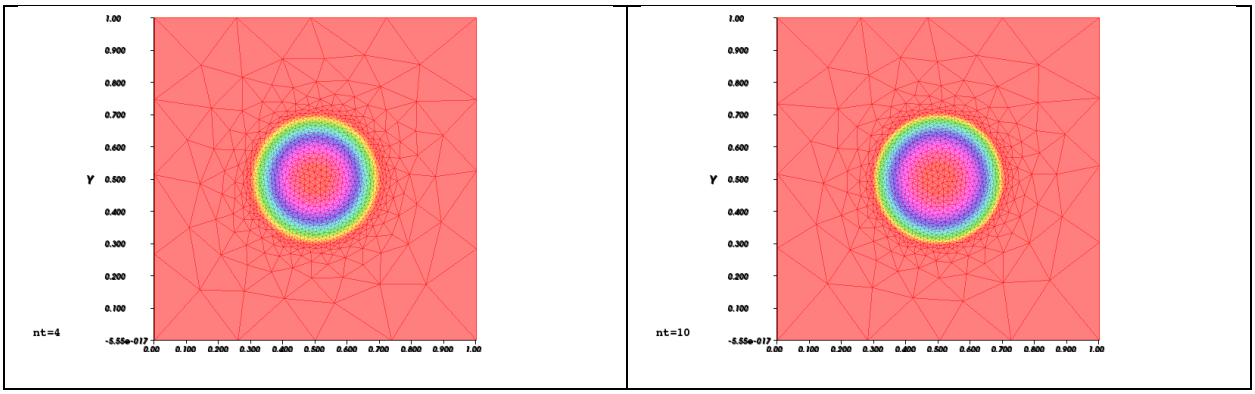

Figure 4.27 No fracture with adaptation, m=2.

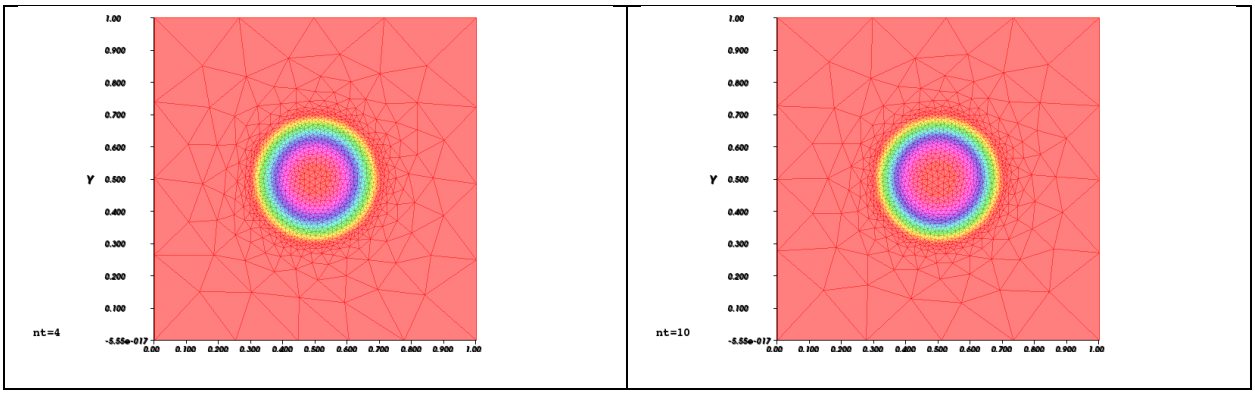

Figure 4.28 No fracture with adaptation, m=5.

As we see in 1D the error using adaptive mesh is smaller than other meshes because most the elements concentrated around the boundary of the support. In Example 9, we can also see the concentration of elements around the boundary (see Figures 4.26, 4.27 and 4.28).

4.2.2.2 Example 10. In this example we consider adaptive mesh with fracture. We use the same parameters as in Example 8.

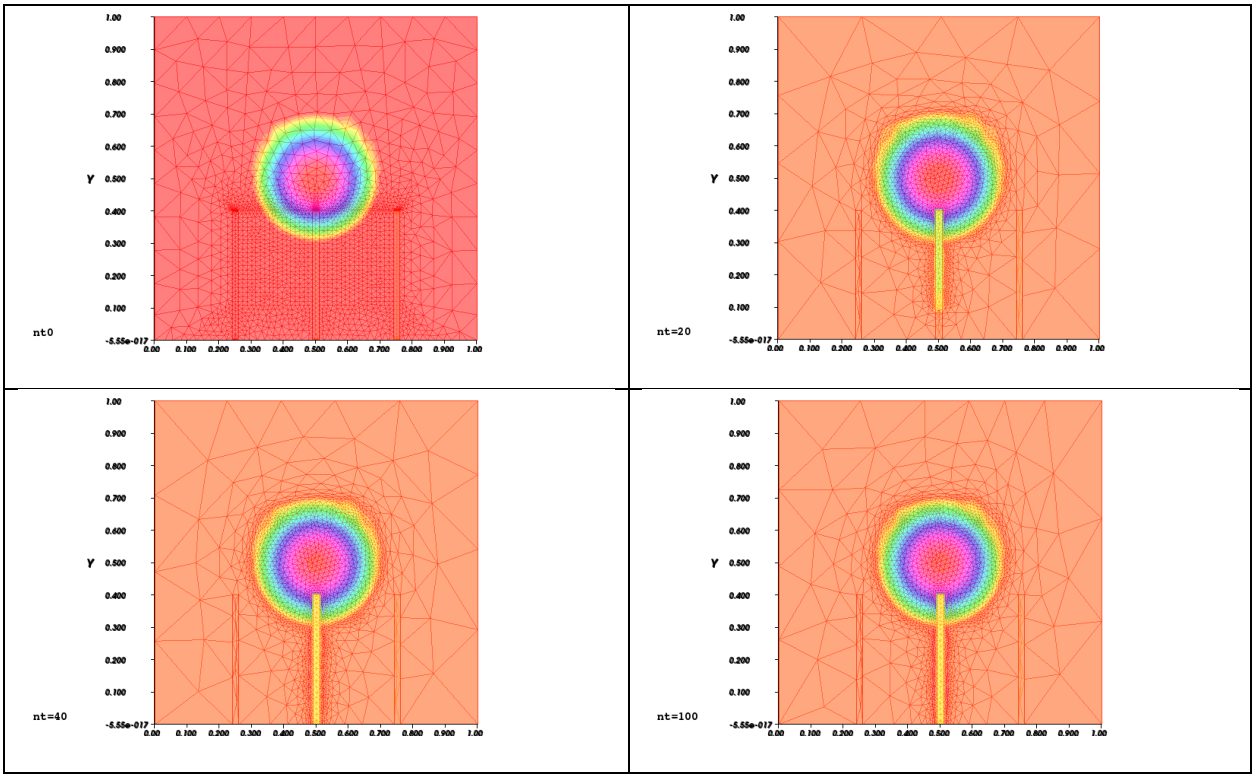

Figure 4.29 Fracture with adaptation, m=1.

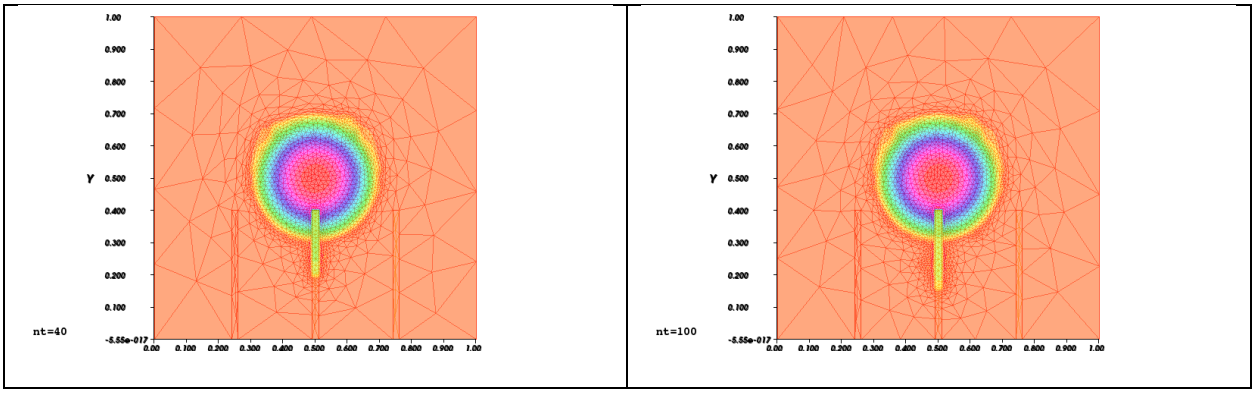

Figure 4.30 Fracture with adaptation, m=2.

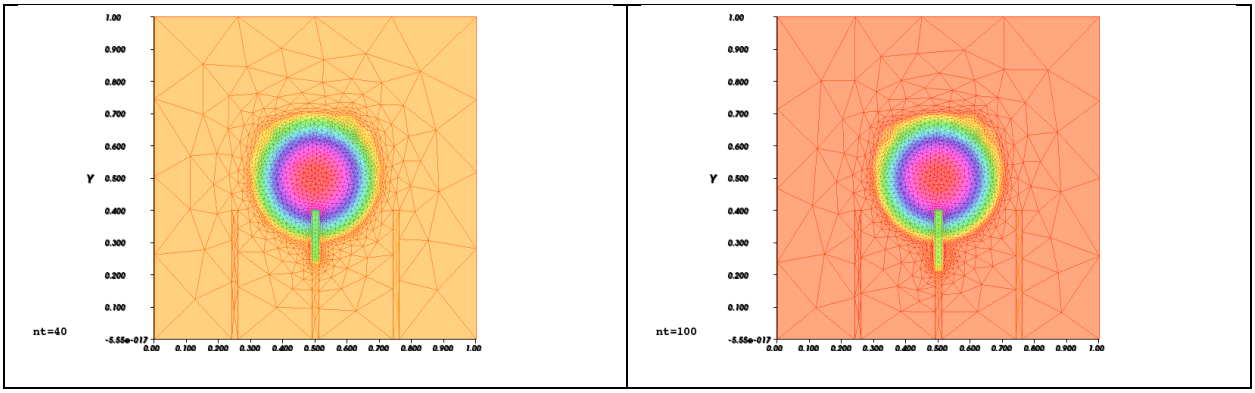

Figure 4.31 Fracture with adaptation, m=5.

In this example, we can see for m=1 and $n_t = 20$ in Figure 4.29, the solution is close to the solution without adaptation in Figure 4.23. Also, when $n_t = 40$ (less than half time) the boundary of support has reached the horizontal well. The mesh elements not only concentrated around the moving boundaries but also around the fractures. The propagation is faster inside the fractures than outside.

CHAPTER 5

CONCLUSION AND SUMMARY

In this thesis, we have conducted simulations to solve the porous medium equation (PME) in fractured reservoirs using Finite Element method and demonstrated the advantages of mesh adaptation in the numerical simulations. We have carried out simulations for both one and two dimensional problems.

For one dimensional problems, we have studied 6 cases, including uniform mesh with and without fracture, adaptive mesh with and without fracture, and log-spacing mesh with and without fracture. We have compared the numerical solutions of the three cases without fracture for different number of elements to the exact analytical solution, and have found that the adaptive mesh gives the best results compared to the other two cases.

In the case of two dimensional problems, we have studied four cases including adaptive mesh with and without fracture, and uniform mesh with and without fracture. We have found that the larger the ratio of the capacity (m) is, the slower the propagation of the solution becomes. We have also observed that the propagation of the solution inside the fracture is faster than the solution outside the fracture. Adaptive mesh also provides better results than the uniform meshes.

In summary, mesh adaptation is an useful tool to improve the efficiency and accuracy in numerical computations, especially for complicated large systems.

References

[1] G. I. Barenblatt, I. P. Zheltov, and I. N. Kochina, "Basic concepts in the theory of seepage of homogeneous liquids in fissured rocks," vol. 24, no. 5, p. 1286-1303, 24 March 1960.

[2] D. T. Snow, "Anisotropie permeability of fractured media," *Water Resour. Res,* vol. 5(6), pp. 1273-1289, 1969.

[3] J. E. Warren, and P. J. Root, "The behavior of naturally fractured reservoirs.," *Society of Petroleum Engineers,* vol. 3, no. 03, p. 245 – 255, 1963.

[4] Y. S. Wu, "On the effective continuum method for modeling multiphase flow, multicomponent transport, and heat transfer in fractured rock.," *Geophys. Monogr. Ser,* vol. 122, p. 299-312., 2000.

[5] J. Boussinesq, "Recherches theoriques sur lecoulement des nappes d'eau infiltres dans le sol," *Comptes Rendus Acad. Sci. / J. Math. Pures. Appl.10,* pp. 5-78., 04 1903.

[6] M. Muskat, "The flow of homogeneous fluids through porous media,," *Journal of Geology 46,* vol. 169, no. 6, pp. 902-903, 1937.

[7] H. Darcy, Les fontaines publiques de la ville de Dijon, Paris: Victor Dalmont Editeur , 1856, pp. 305-401.

[8] J. L. Vazquez, The Porous Medium Equation, Oxford Mathematical Monographs, 2006.

[9] F. Benjamin, Two-phase flow modeling in porous media with kinetic interphase mass transfer processes in fractures., (Master Thesis), 2009.

[10] L. S. Leibenzon, "The motion of a gas in a porous medium, Complete works," *Neftanoe khozyastvo,*, vol. 2, pp. 8-10, 1930.

[11] A. Friedman, Partial deferential equations of parabolic type, Englewood Cliffs, N. J. Parentice-Hall, 1964..

[12] O. A. Ladyzhenskaya, V.A. Solonnikov, and N.N. Ural'tseva., Linear and quasilinear equations of parabolic type, American Mathematical Society, 1968.

[13] J. A. Smoller, Shock Waves and Reaction—Diffusion Equations, Grundlehren der mathematischen Wissenschaften, 1982.

[14] A. Friedman, "Variational principles and free boundaries," *Society for industrial and applied mathematics*, vol. 26, no. 2, pp. 307-308, 1984.

[15] B. Bourbiaux, "Fractured reservoir simulation: a challenging and rewarding," *Oil & Gas Science and Technology* , vol. 65, no. 2, p. 227–238., 2010.

[16] B. Bourbiaux, R. Basquet, M. Cacas, and J. Daniel, "An integrated workflow to account for fractures in multi-scale reservoir simulation models: implementation and benefits," in *Society of Petroleum Engineers*, Abu Dhabi International Petroleum Exhibition and Conference, 2002.

[17] A. Assteerawatt, Flow and transport modelling of fractured aquifers based on a geostatistical approach., (Dissertation), 2008.

[18] V. Martin,J. Jaffré,and J. Roberts, "Modeling fractures and barriers as interfaces for flow in porous media," *SIAM Journal on Scientific Computing,*, vol. 26, no. 5, p. 1667–1691, 2005.

[19] G. J. Moridis, T. A. Blasingame, and C. M. Freeman, "Analysis of mechanisms of flow in fractured tight-gas and shale-gas reservoirs," in *Society of Petroleum Engineers*, Lima, Peru, 2010.

[20] O. M. Olorode, Numerical modeling of fractured shale-gas and tight-gas reservoirs using unstructured grids, (master thesis), 2011.

[21] O. Houze,E. Tauzin, V. Artus, L. Larsen, "The analysis of dynamic data in shale gas reservoirs-part1," company report, Kappa engineering, Houston, Texas, USA, 2010.

[22] H. Kazemi, "Pressure transient of naturally fractured reservoirs with uniform fracture distribution.," *SPEJ*, vol. 9, no. 04, p. 451– 462, 1969.

[23] A. Swaan, "Analytic solutions for determining naturally fractured reservoir properties by well testing.," *Society of Petroleum Engineers*, vol. 16, no. 03, p. 117 – 122, 1976.

[24] E. Ozkan, U. Ohaeri, and R. Raghavan, "Unsteady flow to a well produced at a constant pressure in fractured reservoir," *Society of Petroleum Engineers*, vol. 2, no. 02, pp. 186 - 200, 1987.

[25] R. A. Wattenbarger, "Some reservoir performance aspects of unconventional gas production," in *Private Conference Presentation,*, Lake Louise, Alberta, Canada., 2007.

[26] A. El-Banbi, Analysis of tight gas wells, (Dissertation), 1998.

[27] R. O. Bello, and R. A. Wattenbarger, "Modeling and analysis of shale gas production with a skin effect.," *Journal of Canadian Petroleum Technology*, vol. 49, no. 12, pp. 16-18, 2010.

[28] R.O.Bello, Rate transient analysis in shale gas reservoirs with transient linear behavior., (Dissertation), 2009.

[29] R. O. Bello, and R. A. Wattenbarger, "Rate transient analysis in naturally fractured shale gas reservoirs," in *Gas Technology Symposium*, Calgary, Alberta, Canada,, 2008.

[30] R. O. Bello, and R. A. Wattenbarger, "Multi-stage hydraulically fractured shale gas rate transient analysis," in *North Africa Technical Conference and Exhibition*, Cairo, Egypt, 2010.

[31] E. Ozkan, M. Brown, and H. Kazemi, "Comparison of fractured horizontal-well performance in conventional and unconventional reservoirs.," in *Western Regional Meeting, 24-26 March*, San Jose, California, 2009.

[32] H. A. Al-Ahmadi, A. M. Almarzooq, and R. A. Wattenbarger, "Application of linear flow analysis to shale gas wells – field cases.," in *Unconventional Gas Conference, 23-25 February*, Pittsburgh, Pennsylvania, 2010.

[33] F. Hecht, "New development in freefem++.," *Journal of Numerical Mathematics,* vol. 20, no. 3-4, pp. 251-265, 2012.

[34] J. U. Brackbill and J. S. Saltzman, "Adaptive zoning for singular problems in two dimensions," *Journal of Computational Physics,* vol. 46, no. 3, pp. 342-368, 1982.

[35] A. S. Dvinsky, "Adaptive grid generation from harmonic maps on Riemannian manifolds," *Journal of Computational Physics,* vol. 95, no. 2, pp. 450-476, 1991.

[36] P. M. Knupp and N. Robidoux, "A framework for variational grid generation: conditioning the jacobian matrix with matrix norms," *Journal on Scientific Computing,* vol. 21, no. 6, pp. 2029-2047, 2000.

[37] W. Cao, W. Huang, and R. D. Russell,, "A study of monitor functions for two dimensional adaptive mesh generation," *Journal on Scientific Computing,* vol. 20, no. 6, pp. 1978-1994, 1999.

[38] R.V. Garimella and M.S. Shephard, "Boundary layer meshing for viscous flows in complex domain," in *7th International Meshing Roundtable, pages 107–118,*, Albuquerque, NM, 1998.

[39] S. Yamakawa and K. Shimada, "High quality anisotropic tetrahedral mesh generation via ellipsoidal bubble packing.," in *9th International Meshing Roundtable, pages 263–273,*, Albuquerque, NM, 2000.

[40] H. Borouchaki, P.L. George, and B. Mohammadi., "Delaunay mesh generation governed by metric specification:Part II applications," . *Finite Element in Analysis and Design,* vol. 25, no. 1-2, pp. 85-109, 1997.

[41] H. Borouchaki, P.L. George, F. Hecht, P. Laug, and E. Saletl., "Delaunay mesh generation governed by metric specification Part I. Algorithms," *Finite Elements in Analysis and Design,* vol. 25, no. 1-2, pp. 61-83, 1997.

[42] M.J. Castro-D´ıaz, F. Hecht, B. Mohammadi, and O. Pironneau, "Ansitropic unstructured mesh adaption for flow simulations," *International Journal for Numerical Methods in Fluids,* vol. 25, no. 4, p. 475–491, 1997.

[43] J. Peraire, M. Vahdati, K. Morgan, and O.C. Zienkiewicz., "Adaptive remeshing for compressible flow computations.," *Journal of Computational Physics,* vol. 72, no. 2, p. 449–466, 1987.

[44] W. G. Habashi, J. Dompierre, Y. Bourgault, D. Ait-Ali-Yahia, M. Fortin, and M. Vallet., "Anisotropic mesh adaptation: towards user-independent, meshindependent and solver-independent CFD. Part I: General principles," *International journal for numerical methods in fluids,* vol. 32, no. 6, pp. 725–744,, 2000.

[45] D. Ait-Ali-Yahia, G. Baruzzi, W.G. Habashi, M. Fortin, J. Dompierre, and M.G. Vallet, "Anisotropic mesh adaptation: towards user-independent, meshindependent and solver-independent cfd. part ii: structured grids," *International Journal for Numerical Methods in Fluids,,* vol. 39, no. 8, p. 657 – 673, 2002.

[46] P.S. Heckbert, and F.J. Bossen, "A pliant method for anisotropic mesh generation," in *5th International Meshing roundtable, pages 63 – 74,*, Albuquerque, NM, 1996.

[47] J. Dompierre, M.G. Vallet, Y. Bourgault, M. Fortin, and W.G. Habashi., "Anisotropic mesh adaptation: towards user-independent, mesh-independent and solver-independent CFD. Part III: Unstructured meshes," *International Journal for Numerical Methods in fluids,* vol. 39, no. 8, p. 675 – 702, 2002.

[48] J. Remacle, X. Li, M.S. Shephard, and J.E. Flaherty, "Anisotropic adaptive simulation of transient flows using discontinuous Galerkin methods," *International Journal for Numerical Methods in Engineering.,* vol. 62, no. 7, pp. 899–923,, 2004.

[49] E.F. D'Azevedo and R.B. Simpson, "On optimal triangular meshes for minimizing the gradient error.," *Numer. Math.,* vol. 59, no. 1, pp. 321 – 348,, 1991.

[50] W.Huang, "Metric tensors for anisotropic mesh generation.," *Journal of Computational Physics,* vol. 204, no. 2, p. 633–665, 2005.

[51] W. Huang, "Mathematical principles of anisotropic mesh adaptation," *Comm Comput. Phys,* vol. 1, p. 276 – 310, 2006.

[52] W. Huang and R.D. Russell, Adaptive Moving Mesh Methods, Springer, New York, 2011.

[53] E. F. D'Azevedo, "Optimal triangular mesh generation by coordinate transformation," *SIAM J. Sci. Stat. Comput.,* pp. 12, 755, 1991.

[54] Ya. B. Zel'dovich, Yu.P. Raizer,, "Physics of Shock Waves and High-Temperature Hydro-dynamic Phenomena II," *Academic Press,* 1966.

[55] F.hetch, Free Fem++, Paris: Laboratoire Jacques-Louis Lions, Universite Pierre et Marie Curie.

[56] E. Ozka, U. Ohaeri, and R. Raghavan, "Unsteady flow to a well produced at a constant pressure in fractured reservoir.," *Society of Petroleum Engineering,* vol. 14, no. 02, 2011.

VITA

Ahmed Azeez was born in Kirkuk, Iraq on May 2, 1987. He completed his Bachelor's Degree (B.Sc.) in Mathematics from Tikrit University, Tikrit, Iraq in 2010. He worked as a teaching assistant at the Mathematics Department/ College of computer Science and Mathematics/Tikrit University after he received his Bachelor's degree.

He received HCED (Higher Committee for Educational Development in Iraq) Scholarship award to the University of Missouri – Kansas City, USA and started his Master's Degree in Mathematics in January 2016.